THESIS ON MECHANICAL AND INSTRUMENTAL ENGINEERING E42

FATIGUE CHARACTERISTICS OF PM STEELS

MART SAARNA

TALLINN UNIVERSITY OF TECHNOLOGY
Faculty of Mechanical Engineering
Department of Materials Engineering

Dissertation was accepted for the defence of the degree of Doctor of Philosophy in Engineering on 27. 06. 2008

Supervisor: Prof. Priit Kulu, Department of Materials Engineering, Tallinn University of Technology

Opponents: Prof. Michal Besterci, Institute of Materials Research, Slovak Academy of Sciences, Košice, Slovakia

Assoc. prof. Priit Põdra D.Eng, Department of Mechatronics, Tallinn University of Technology

Defence of the thesis: 11.09.2008, at 11:00
Room no.: V – 215
Tallinn University of Technology
Ehitajate tee 5, Tallinn, Estonia

Declaration

Hereby I declare that this doctoral thesis, my original investigation and achievement, submitted for the doctoral degree at Tallinn University of Technology has not been submitted for any academic degree.

/töö autori nimi ja allkiri/

Copyright: Mart Saarna, 2008
ISSN 1406-4758
ISBN 978-9985-59-841-2

MASINA- JA APARAADIEHITUS E42

PULBERTERASTE VÄSIMUSKARAKTERISTIKUD

MART SAARNA

CONTENTS

INTRODUCTION 7
ABBREVIATIONS, TERMS AND OF SYMBOLS 9
1 REVIEW OF THE LITERATURE 11
1.1 Fatigue of materials 11
1.1.1 Fatigue – principle 11
1.1.2 Fatigue data presentation 13
1.1.3 Fatigue data scattering 15
1.1.4 Prediction of steels fatigue life 15
1.1.5 Duplex stainless steels 20
1.2 Fatigue at wear 22
1.2.1 Fatigue strength of wear resistant material 22
1.2.2 Fatigue *vs*. abrasive wear resistance 23
1.3 Conclusions to the chapter 24
1.4 Aims of the study 24
2 EXPERIMENTAL 25
2.1 Materials to be tested 25
2.1.1 Duplex stainless steels 25
2.1.2 Wear resistant materials 32
2.2 Test methods 33
2.2.1 Corrosion fatigue testing 33
2.2.2 Surface fatigue testing 35
2.2.3 Abrasive wear testing 36
2.2.4 Fractography and topography studies 37
3 RESULTS AND DISCUSSION 38
3.1 Corrosion fatigue testing 38
3.1.1 Fracture surface analysis 45
3.2 Surface fatigue wear testing 47
CONCLUSIONS 51
REFERENCES 53
LIST OF PUBLICATIONS 58
ABSTRACT 60
KOKKUVÕTE 61
CURRICULUM VITAE 64
ELULOOKIRJELDUS 66

INTRODUCTION

In European materials programs great attention is focused on composite materials, including nano- and wear resistant materials, *etc*. Among the priorities in engineering materials for challenging applications, understanding the degradation mechanism of materials is noted in the European Technology Platform for Advanced Engineering Materials and Technologies (EuMAT).

Often the reasons for failure of machine parts and components often lie behind corrosion and wear, as well as fatigue. In most of the cases, the following combined processes occur: wear-corrosion, corrosion-fatigue and wear-fatigue. Loss of material due to combined effects of corrosion, wear and fatigue has received much attention in recent years, due to the prevalence of such problems in many diverse environments such as seawater, white water *etc*.

For protection against corrosion stainless steels are used, among them duplex stainless steels (DSS) are used. DSS are excellent in corrosion resistance but their behaviour in fatigue has been studied less. The problem of determining the fatigue strength of duplex steels and wear resistant materials is significant both from the theoretical and practical point of view. In case of duplex steels, determination of the fatigue performance at different stress levels and in corrosive is important in predicting the life expectancy of a part manufactured from that steel. This is the case, for example, in pulp and paper industry where duplex steels are used for manufacturing the suctions rolls. Suction rolls are used at the wet end of the paper machine to remove the white water from the paper. In order to remove the white water, holes are drilled into the suction roll shells, which serve as stress raisers. Suction rolls are subjected to cyclic stress accompanied by corrosive environment. This can lead to failure by corrosion fatigue. DSS have proven to be superior to conventional stainless steels in pulp and paper industry due to their good corrosion resistance and mechanical strength. This is achieved by the ferritic- austenitic double structure of the duplex steels.

Most commercial grinding appliances, working in abrasive wear conditions today, are produced from high manganese and chromium steels because of their ability to withstand severe impact conditions such as those experienced in ball mills. The main advantages of the above-mentioned steels are their adaptability to most milling conditions and their favourable cost to wear ratios. Prospective tribological materials are typical of heterogeneous structure – hard particles in a relatively soft matrix. For abrasive wear conditions, metal-matrix composites (MMC) are preferred. This kind of carbide containing materials and coatings produced by powder metallurgy (PM) and thermal spray methods are widely used in many applications demanding wear, corrosion and impact resistance. Putting aside the excellent abrasive wear resistance of MMC, behaviour in conditions of fatigue has not been investigated. As a rule, similar materials at extreme conditions of abrasive wear (high velocities, impact loading *etc*.) have low wear resistance probably due to the low fatigue strength.

In abrasive wear, two different mechanisms of material removal occur either separately or simultaneously. At abrasion and low-angle abrasive erosion, microcutting dominates, and the main criterion for materials selection is hardness.

At high angle impact as well as at oblique impact by irreversible deformation, the exposed surface should be able to withstand repeated deformation, where low-cycle fatigue mechanism dominates. Hence the fatigue performance and mechanism for wear resistant materials, such as metal-matrix composites for example, needs to be characterized.

Current thesis is based on four main publications.

Acknowledgements

The research at hand was carried out mainly in the Department of Materials Engineering of Tallinn University of Technology and partially in Department of Materials Science Tampere University of Technology and as a part of contract between the Department of Materials Engineering of Tallinn University of Technology and Metso Corporation Finland. The research was supported by the Estonian Science Foundation (grant No. 5581)

Firstly I would like to express my gratitude to my supervisor Prof. Priit Kulu for his support, guidance and most of all patience in supervising my studies and thesis writing and making it possible for me to carry out my research.

I would like to thank Prof. Veli-Tapani Kuokkala, for giving me the opportunity to carry out my research, and MSc. Mikko Hokka for helping me to conduct the tests at Tampere University of Technology and Mr. Pekka Siitonen from Metso Corporation for being a patient and understanding research partner.

My gratitude goes also to my colleagues at Department of Materials Engineering of Tallinn University of Technology, especially Prof. Renno Veinthal, PhD Lauri Kollo, PhD Fjodor Sergejev, PhD Priidu Peetsalu and PhD student Riho Tarbe for their comments and support, PhD Mart Viljus from the Centre of Material Research for helping me to carry out the fractography study and characterization of microstructure as well as the staff and students at the Laboratory of Mechanical Testing and Metrology of Tallinn University of Technology for supporting me with my experiments.

Finally I would like to thank my family for their unconditional support and encouragements during my studies and thesis writing.

ABBREVIATIONS, TERMS AND OF SYMBOLS

$\sqrt{area}$ – Murakami parameter
A – amplitude ratio
AEW – Abrasive Erosion Wear
AIW – Abrasive Impact Wear
b – fatigue strength exponent (Basquin exponent)
C/P – cycles per point
C_D – size factor
C_L – loading factor
C_R – reliability factor
C_S – surface finish factor
da/dn-ΔK – fracture mechanics parameters
DSS – Duplex Stainless Steel
EDS – Energy Dispersive Spectrometer
HCF – High-Cycle Fatigue
HIP – Hot Isostatic Pressing
HV – Vickers hardness number (followed by load)
I_v – volumetric wear rate, mm^3 / kg
LCF – Low-Cycle Fatigue
LOM – Light Optical Microscope
MMC – Metal Matrix Composite
N – cycle number
N_f – cycles to failure
pH – measure of the acidity or alkalinity of a solution.
PM – Powder Metallurgy
ppm – parts per million, mg / l
PRE – Pitting Resistance Number
PREN – Pitting Resistance Number including nitrogen
R – stress ratio
Ra – average surface roughness, μm
R_m (S_u) – tensile strength, MPa
S'_f – fatigue strength coefficient
$S_{0.2y}$ ($R_{po.2}$) – offset yield at 0.2% non proportional elongation, MPa
S_{1000} – fatigue strength at 10^3 cycles, MPa
S_a (S_{alt},σ_a) – alternating stress, MPa
S_{ar} – fully reversed stress amplitude for a given fatigue life (cycles)
S_{be} – base line fatigue strength, MPa
S_{cr} – completely reversed stress amplitude for a given fatigue life, MPa
SDSS – Super Duplex Stainless Steel
S_e (σ_e) – fatigue (endurance) limit fully reversed loading R = –1, MPa
SEM – Scanning Electron Microscope
S_f (σ_f) – fatigue strength, MPa
SFW – Surface Fatigue Wear, mm^3

S_{max} – maximum stress, MPa
S_{mean} (S_m) – mean stress, MPa
S_{min} – minimum stress, MPa
S-N – stress *vs.* cycles curve (stress-life diagram)
S_y – yield strength, MPa
UHCF – Ultra-High-Cycle Fatigue
vol% – volume percent
wt% – weight percent
α – ferrite
γ – austenite
Δσ – stress range, MPa
ε-N – strain *vs.* cycles curve (strain-life diagram)
ε_v – relative wear resistance
σ_w – fatigue limit in case of small defects (Murakami), MPa
σ_{wo} – fatigue limit (Murakami), MPa

1 REVIEW OF THE LITERATURE

1.1 Fatigue of materials

1.1.1 Fatigue – principle

Fatigue is a progressive, localized, permanent structural change that occurs in materials when subjected to fluctuating stresses and strains that may result in development of cracks or fracture after a sufficient number of cycles or fluctuations [1].

During cyclic stressing or straining which lead to inelastic deformation, the metal can either lead to cyclical softening, hardening or, in some case, become cyclically stable. When a metal is initially soft the dislocation density is low. As a result of inelastic deformation the dislocation density grows, which decreases their mobility, – the metal becomes cyclically hardened. For metals that are initially hard or have been hardened the inelastic strain causes rearrangement of the dislocation structure that leads to softening. The rearrangement also enhances the dislocation mobility and dislocations are able to circumnavigate around microstructural barriers that generally tend to restrict deformation, such as precipitates and grain boundaries [2].

Notches, inclusions and cracks can lead to an increase in local stress or strain levels up to the point of inelastic deformation and also cause local cyclic softening or hardening [2, 3]. This is due to the crystallographic nature of the metals and the presence, density and movement of dislocations. Dislocations, when moving along the crystallographic planes, form slip bands along which a slip occurs (about 0.1 μm in width) *i.e.* an inelastic deformation occurs [2].

The crack nucleation mechanism varies depending on the ductility *i.e.* the movement of the dislocations in metals. Slipbands intrusions form stress concentrations, can act as a starting point for a crack [2–4]. This can also be said about pitting marks, scratches, inadequate surface roughness etc. [5, 6]. In [7] it is found that the short crack nucleation in duplex steel depends also on the strain level. At high stress levels, slip marks are observed in austenite but not in ferrite – after one third of fatigue life secondary cracks initiate at ferrite [8, 9].

The early stages of fatigue are primarily surface phenomena and thus the surface condition and the environment play a significant role in fatigue performance of a material (Fig. 1.1).

Fatigue cracks may also nucleate at or near the surface discontinuities like inclusions, second phase particles, pores and corrosion pits *etc*., which cause non-uniform stresses in the material [2, 3].

Crack propagation is dived into two stages: I-stage (shear mode) – the microcrack propagates along the shear planes, II-stage (tension) – the crack propagates perpendicular to the loading direction [2].

The formation of fatigue surface markings and striations is schematically shown on Fig. 1.2.

The factors that influence the fatigue performance of a material are [1– 4]:

- loading scheme;
- surface finish;
- environment;
- cyclic frequency;
- mean stresses;
- inclusion content and distribution.

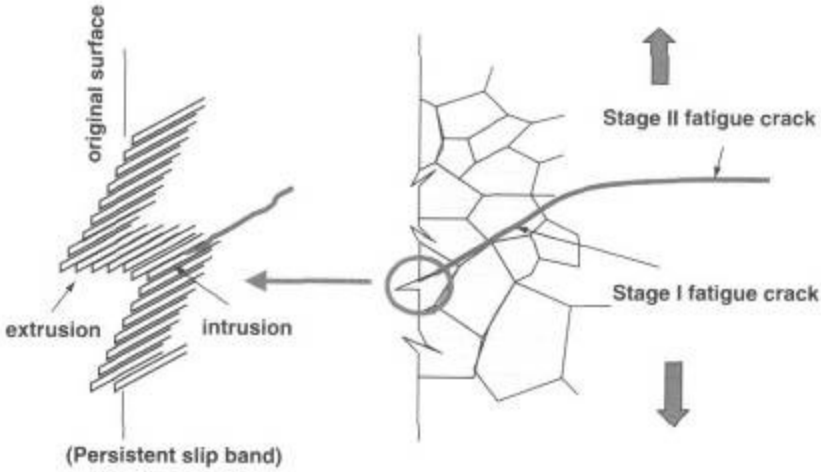

Figure 1.1 Fatigue crack nucleation and propagation during cyclic loading [6]

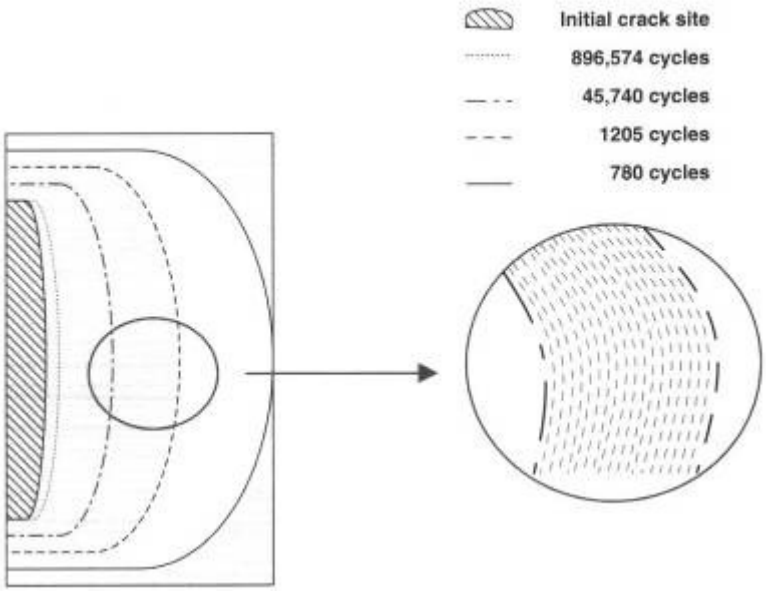

Figure 1.2 Fracture surface markings and striations [6]

Fatigue testing can be carried out in several control regimes – stress control and strain control [10]. The former is used in case of high-cycle fatigue, the latter in case of low-cycle fatigue. There are several loading types possible: axial, torsion, plane bending and rotating bending [2, 11, 12].
For surface fatigue testing, indentation and impression method can be used [13]. Indentation fatigue testing can be carried out with several shapes of indentors, but flat cylindrical indentors allow better characterization of the material since the contact area between the indentor and materials remains constant [14, 15]. To test the surface fatigue properties of wear resistant materials, new test systems have been developed in Tampere University of Technology [17] and in Tallinn University of Technology [18]. The main problem has been defining the failure criterion or having quantative test data [18–20]. The test system developed in Tampere University of Technology enables some quantative analysis of test results.

On the basis of rotating bending fatigue test scheme rolling and sliding friction and fretting fatigue testing can be carried out [16].

1.1.2 Fatigue data presentation

The presentation of fatigue data depends on the design philosophy and methodology as shown in Table 1.1. The typical S-N curve (Wöhler curve) for different environmental conditions for a material possessing a fatigue limit in a non-corrosive environment is shown in Fig. 1.3. Usually logarithmic scale is used for the number of cycles. In case of carbon and low alloy steels the line on the S-N curve appears to become flat at certain point and stress level. This is called a fatigue limit or endurance limit S_e (σ_e) – *i.e.* a stress level at which an infinite number of loading cycles on a smooth and notch free specimen is possible [4]. On the other hand, in case of non-ferrous alloys and a corrosive environment, the curve does not approach as an asymptote and only finite numbers of cycles at certain stress level can be obtained. This is called fatigue strength S_f (σ_f) [3, 6, 21].
At short fatigue lives, up to 10^4 cycles, and high yielding stress level noticeable plastic deformation occurs and the fatigue crack propagates quite rapidly. This is called *low-cycle fatigue* (LCF). In case of LCF usually strain controlled testing is carried out and thus strain-life approach is used. The fatigue data obtained in case when yielding stress is not dominant is called *high-cycle fatigue* (HCF) from 10^4 up to 10^7 cycles. Testing is carried out under stress control and stress-life approach is used. When cycles are $>10^7$ it is referred to as *ultra-high cycle fatigue* (UHCF) and testing is carried out, as was the case with HCF [1].

From Figure 1.3 it can be seen that the best results can be obtained in vacuum, in which fatigue limit at run out are obtained. In case of a corroding sample, only fatigue strength can be obtained at different stress levels.

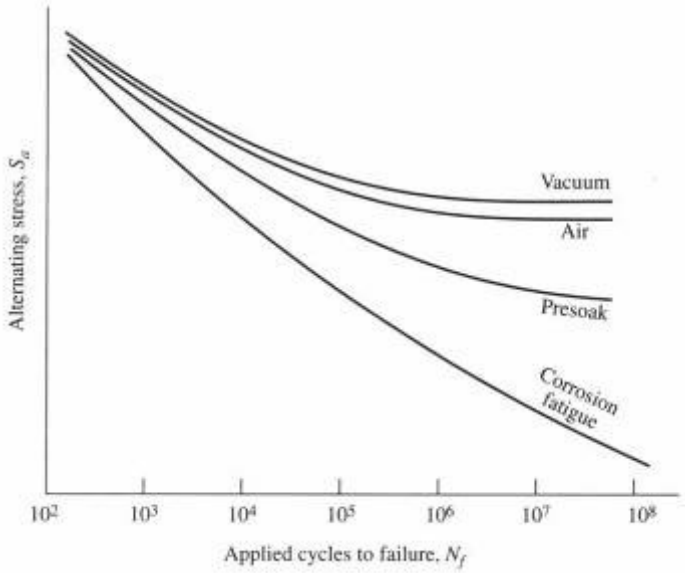

Figure 1.3 Relative S-N curves of fatigue behaviour under various environmental conditions [2]

Table 1.1 Fatigue data representation according to the design philosophy [1]

Design philosophy	**Design methodology**	**Principal testing data description**
Safe life, infinite life	Stress-life	S-N
Safe life, finite life	Strain-life	ε-N
Damage tolerant	Fracture mechanics	da/dn-ΔK

Since the research is carried out using stress-life approach in this work a stress loading cycle parameters will be discussed. They are as follows [3, 6]:

- maximum stress S_{max} (σ_{max});
- minimum stress S_{min} (σ_{min});
- stress range/stress amplitude S_r ($\Delta\sigma$) $= S_{max} - S_{min}$;
- alternating stress S_a (σ_a) ;
- mean stress S_m (σ_m) $= (S_{max} + S_{min})/2$;
- stress ratio $R = S_{min}/S_{max}$;
- amplitude ratio $A = S_a/S_m$.

The graphical interpretation of stresses is given in Fig. 1.4. Usually sinusoidal form of loading is used however in case of rotating bending only sinusoidal form is possible.

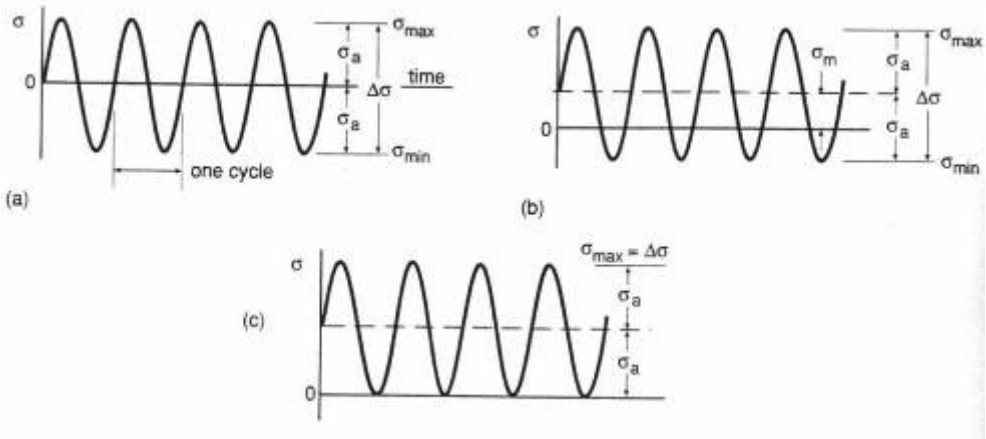

Figure 1.4 Constant amplitude cycles: a — fully reversed; b — tensile mean stress; c — zero-to tension [3]

1.1.3 Fatigue data scattering

Usually, during fatigue testing, considerable statistical scatter exists. When testing cycles to failure N_f usually a skewed distribution occurs. However, when log N_f is used as the variable then usually a log-normal or Weibull distribution of N_f is achieved [3]. 50% probability of survival is used [21–23].
Scattering is mainly caused by the test scheme (frequency of cycling, temperature, environment *etc.*) but also by the preparation of the specimen (surface finish, residual stresses *etc.*) [3, 10, 21, 23].

1.1.4 Prediction of steels fatigue life

In order to roughly estimate the fatigue life and hence predict the stress levels in order to plan the testing two parameters should be obtained – fatigue strength at 10^3 cycles and base line bending fatigue strength at 10^6 cycles.

Prediction of fatigue strength at 10^3 in case of axial loading.
In case of 10^3 cycles the effect of size and surface are not important [2, 6].
The fatigue strength at 10^3 cycles (S_{1000}) depends on the reliability level (C_R) and type of loading as follows [6]:
$S_{1000,\ R} = S_{1000} \times C_R,$, (1.1)
where: C_R value with 95 confidence level is 0.868.
For axial loading the $S_{1000} = 0.75 \times S_u$. (1.2)

Prediction of the fatigue at 10^6 in absence of major defects
General relationship between fatigue limit at 10^6 cycles and tensile strength for polished, notched and corroding steel specimens is given in Fig. 1.5.

Base line bending fatigue strength S_{be} at 10^6 cycles for a highly polished steel specimen can be roughly estimated from ultimate tensile strength S_u (R_m) as follows [3]:

$$S_{be} \approx S_u/2, \quad \text{for } S_u \leq 1400 \text{ MPa}. \tag{1.3}$$

For high strength steels and non-ferrous metals at 10^8 cycles [1, 2]:

$$S_{be} \approx S_u/3; \tag{1.4}$$

$$S_{be} \approx 700 \text{ MPa}, \quad \text{for } S_u \geq 1400 \text{ MPa}. \tag{1.5}$$

In order to predict fatigue limit several empirical factors need to be accounted for:

$$S_f(10^6 \text{ cycles}) = S_{be} \times C_L \times C_S \times C_D \text{ x } C_R \text{ [3, 6]}, \tag{1.6}$$

where: C_L – loading factor (0.75 – 0.90 in case of axial loading); C_S – surface finish (1.0 mirror polished surface); C_D – size (1.0 in case of axial loading and d < 8 mm); C_R – reliability level (1.0 for estimation).

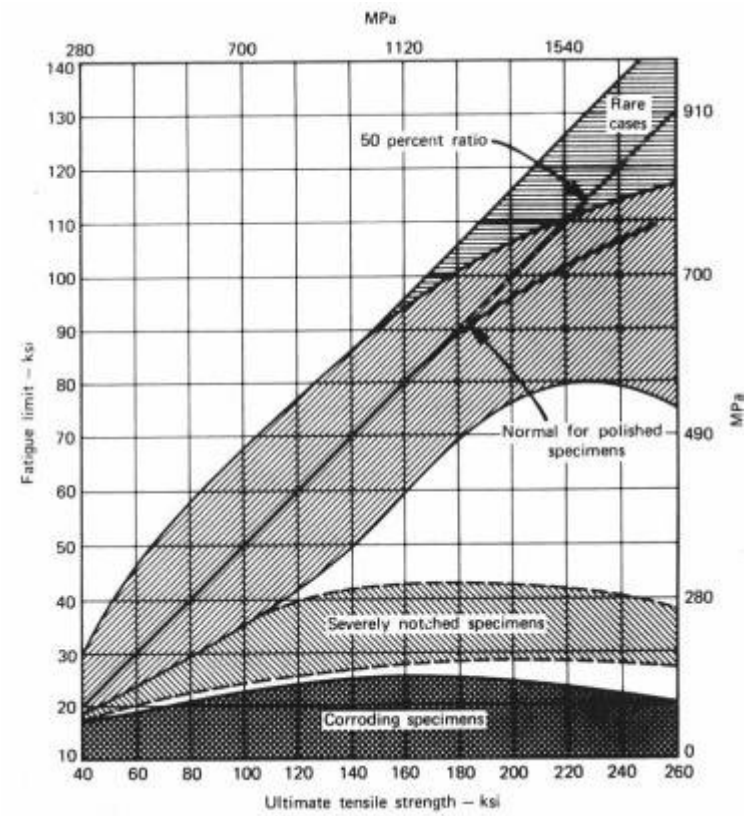

Figure 1.5 General relationships between fatigue limit and tensile strength for polished, notched and corroding steel specimens [2, 11]

Murakami has proposed a formula predicting the fatigue limit of (10^7 for steels) relatively pure ferrous materials by the Vickers hardness [4]:

$$\sigma_{wo} = 1.6 \text{ HV} \pm 0.1 \text{ HV (for HV} < 400). \tag{1.7}$$

Fatigue limit can be also estimated by using Brinell hardness number [1]:

$S_{be} = 0.25 \times HB$ (for HB < 500). (1.8)

However all the proposed equations should be seen as estimates.
It is also worth mentioning that rotating bending gives significantly longer lives compared to axial testing, especially at high stress levels [1].

Fatigue data presentation
If fatigue data approximates a straight line on a log-log plot, the following equation represents the curve [3, 6]:

$$S_f = S'_f (2N_f)^b, \quad (1.9)$$

where: S'_f (fatigue-strength coefficient) and b (fatigue strength exponent, Basquin exponent) are fitting constants based on un-notched specimen with completely reversed loading $S_m = 0$. The S'_f can be estimated as follows:

$$S'_f = (S_u + 50), \quad \text{for steels about 500 HB} \quad (1.10)$$

The fatigue strength exponent is usually between (−0.05) − (−0.12). For most metals the average is −0.085 [1].
One possibility to predict the fatigue limit in case of mean stresses is by Eq. (1.11) [1]:

$$S_f = (S'_f - S_m)(2N_f)^b \quad (1.11)$$

Murakami method for prediction of fatigue limit in presence of small defects
According to Murakami not all cracks propagate once they have initiated. Some cracks nucleate and then stop as long as the fatigue limit is not passed. In light of that he proposed a more precise definition to fatigue for unnotched specimen fatigue limit is the threshold stress for crack propagation. This implies that the presence of defects such as cracks, pores non-metallic inclusion does not necessarily lead to fracture [4].
The effect of non-metallic inclusions is similar to small defects [4]. Murakami has proposed a method for estimating the fatigue strength of an alloy containing defects such as non-metallic inclusions based on the Vickers hardness number and the square root of the defect area $\sqrt{area}$ that is measured perpendicular to the maximum principal stress [4] as follows:

by surface inclusion

$$\sigma_w = 1.43(HV+120) / \sqrt{area}^{\,1/6}; \quad (1.12)$$

just below surface inclusion

$$\sigma_w = 1.41(HV+120) / \sqrt{area}^{\,1/6}; \quad (1.13)$$

by interior inclusion

$$\sigma_w = 1.56(HV+120) / \sqrt{area}^{\,1/6}. \quad (1.14)$$

In case of asymmetrical loading where $R \neq -1$ the fatigue limit can be estimated as follows [4]:

by surface inclusion

$\sigma_w = [1.43(HV + 120)/ \sqrt{area}^{1/6}] [(1 - R)/2]^{\alpha}$; (1.15)

just below surface inclusion

$\sigma_w = [1.41(HV + 120)/ \sqrt{area}^{1/6}] [(1 - R)/2]^{\alpha}$; (1.16)

by interior inclusion

$\sigma_w = [1.56(HV + 120)/ \sqrt{area}^{1/6}] [(1 - R)/2]^{\alpha}$, (1.17)

where: $\alpha = 0.226 + HV \times 10^{-4}$ and the units are: σ_w – MPa, HV – kgf/mm^2, $\sqrt{area}$ – μm.

These estimations can be used when the $\sqrt{area}$ is less then 1000 μm. In case of stress levels below the fatigue limit, only the $\sqrt{area}$ is enough to predict the fatigue limit. However above the fatigue limit, the geometry of the defect is also important [4]. Murakami approach can be also used to predict fatigue limit of surface hardened steels [24].

Mean stress effect

It is widely known that tensile mean stresses decease and compressive mean stresses increase the fatigue life of a component. Mean stresses on a surface layer have similar effects. One explanation for latter is that cracks tend to grow in tension. This has led to crack-closure investigations. Crack-closure is caused by compressive loads, surface roughness of a crack, plastic deformations behind and ahead of a crack. Usually these are made in strain control using compact tension specimens, however but stress control and standard fatigue specimen is also possible [25–27].

The mean stress effect is demonstrated in Fig. 1.6. At intermediate or high mean stress levels during load control test, substantial cyclic creep can occur. This adds to the detrimental effects of tensile mean stresses [2].

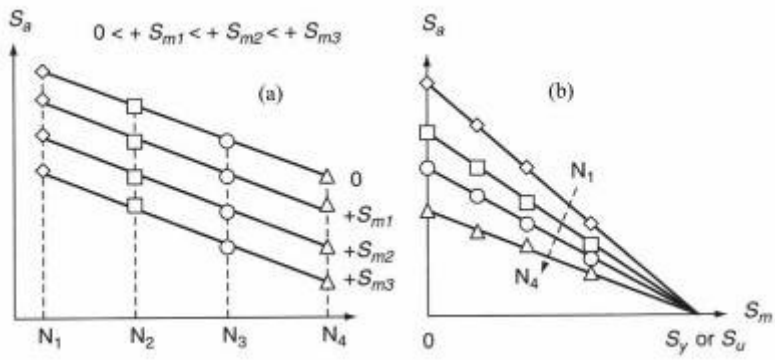

Figure 1.6 Mean stress effect on fatigue life: a – S-N curve at constant mean stress; b – constant life diagram [6]

It is possible to predict if the metal will cyclically soften or harden as follows [1]:

$S_u/S_{0.2y} > 1.4$ (hardening expected); (1.18)
$S_u/S_{0.2y} < 1.2$ (softening expected), (1.19)
where: $S_{0.2y}$ is offset 0.2 % yield strength.
Between 1.2 –1.4 metal is stable or may harden or soften.

In case of tensile mean stresses initial cyclic hardening can be followed by cyclic softening, at symmetrical loading only cyclic softening is observed in 9% Cr-1% Mo steel [28]. Also exponential stress function can be used in order to predict the fatigue strength in presence of mean stresses [29].

In order to find out how the mean stresses influence the fatigue life at certain mean stress levels the data could be presented in many ways out of which the S-N and constant life diagrams are mostly used [10]. The data presented in a S-N form are shown in Fig. 1.6a. A constant life diagram is shown in Fig. 1.6b. This is done by taking points from the S-N curves at various cycle counts and then plotting combinations of stress amplitude and mean stress for those cycle count. The most used is S_m *vs.* S_a diagram (Haigh plot) – which allows predicting of the S_m and S_a values for a given constant cycle number (Table 1.2) [1–3, 6].

Table 1.2 Equations for constant life diagram.

Model	**Equation**	**Designation**
Goodman	$\frac{S_a}{S_{cr}} + \frac{S_m}{S_u} = 1$ (1.20)	Linear, best suited for relatively low ductile materials
Gerber	$\frac{S_a}{S_{cr}} + \left(\frac{S_m}{S_u}\right)^2 = 1$ (1.21)	Parabola, best suited for smooth or notched ductile materials.
Soderberg	$\frac{S_a}{S_{cr}} + \frac{S_m}{S_y} = 1$ (1.22)	Very conservative in most cases

Corrosion fatigue of steels

Corrosion fatigue is caused by crack development under simultaneous action of corrosion and fluctuating or cyclic stress. The damage due to corrosion fatigue is almost always greater than the sum of damage by corrosion and fatigue acting separately. Corrosion fatigue cracks tend to initiate at surface discontinuities, such as notches and pits [30].

In case of corrosion fatigue there is no apparent fatigue limit (Figs. 1.3 and 1.5) [30]. This is caused by overall corrosion, pitting corrosion and more pronounced material dissolution at crack tip and hydrogen embrittelement. A corrosive environment can influence all the stages of crack development except the last one, in which ductile fracture occurs. Corrosion fatigue cracks can be transgranular, intergranular or a combination of both, depending on the mechanical loading and environmental conditions [21, 30].

The testing frequency is an important factor unlike testing in air where testing frequency has little effect [21, 30]. This can also be seen in Fig. 1.3. This is due to the fact that corrosion needs time to occur and lead to material degradation.
The results also depend on the way the corrosive environment is applied. Usually submerging the specimen leads to increase in corrosion fatigue strength due to the more restricted oxygen access to the specimen surface and subsequent oxidation [3].

Mean stresses have an effect on corrosion fatigue which is similar to that in non-corrosive environment [2]. The role of inclusions depends on the presence or absence corrosive environment. In the air the harmful inclusions are single phase Al_2O_3, spinels and calcium-aluminates > 10 μm in size. Elongated sulfide inlusions (MnS) appear to be less harmful. On the other hand in a corrosive environment hydrogen sulfide (H_2S) and H-ions formed by dissolution of sulfides have the most deleterious effects on the development of corrosion pits. For an inclusion to be a potential source of fatigue failure, two main criteria must be fulfilled: the inclusion should have a critical size and the inclusion should have a low deformability, related to the expansion coefficient at the temperature during fatigue. In high strength steels the fatigue life was dominated by crack initiation, which was due to time, as well as by corrosion pits, which developed by selective dissolution of MnS inclusions [30].

1.1.5 Duplex stainless steels

Duplex stainless steel (DSS) is defined as steel with an austenitic-ferritic structure, with at least 25 or 30% of the smaller phase [30].
In pulp and paper industry DSS-s are prime candidates for use in paper machine suction roll shells [31]. Suction rolls are used in “white water” removal and to control the wet paper web during the paper making process [2]. “White water” is a corrosive environment containing chloride (Cl^{-1}), thiosulphate ($S_2O_3^{2-}$) and sulphate (SO_4^{2-}) ions [25, 32, 33].

DSS are also used as storage tanks, pressure vessels, pipes and tubes [30]. They are manufactured as forged, cast, wrought and powder metallurgy (PM) products. They contain approximately equal separate volume fractions of ferrite *(α)* and austenite *(γ)*, which grant them unique corrosion resistance along with good mechanical properties, which are not affected by the thickness of the specimen or the orientation of microstructure in fully dense PM HIP-ed (Hot Isostatic Pressing)-ed DSS [34, 35]. The good mechanical strength of low-nitrogen DSS originates from the ferrite phase and the high impact toughness from the austenite phase compared to conventional austenitic stainless steel [34]. DSS contain nickel to stabilize the austenite and to form a duplex structure, chromium to give them corrosion resistance and stabilise ferrite, molybdenum to enhance corrosion resistance and stabilize ferrite, nitrogen and manganese to stabilize austenite [36]. Nitrogen is almost completely dissolved in the austenite [34].

Corrosion fatigue resistance of duplex stainless steels

Stainless steel corrosion can be described as a two-step process: initiation and propagation. Resistance to the initiation, which is the breakdown of the passive film, depends mainly on the content of chromium and molybdenum. It is the resistance to the initiation of the corrosion that usually determines if a stainless steel is resistant or not. The nickel content of stainless steel influences propagation, or the rate of which the corrosion attack grows in depth. The low nickel content of the duplex grades can be a disadvantage compared to the austenitic grades, when exposed to media causing uniform corrosion [30].

DSS have excellent resistance to stress corrosion cracking compared to conventional austenitic stainless steels, fatigue cracks tend to grow in ferrite and austenite phase tends to retard the crack [34]. This can be explained by the alloying elements especially chromium, molybdenum and nitrogen and unique behaviour and portioning of the alloying elements of the two phases [34].

When testing DSS in corrosive environment the fatigue crack could initiate at the pitting marks, which could act as stress concentrators. Pitting marks occur when localized corrosion takes place. Resistance to pitting corrosion can be evaluated by the pitting corrosion resistance equivalent (PRE), which is calculated in literature [37] according to Eq. (1.23).

$$PRE = wt\%\ Cr + 3.3\ (wt\%\ Mo) \qquad (1.23)$$

In the case when nitrogen is also present, a PREN value is obtained according to Eq. (1.24).

$$PREN = wt\%\ Cr + 3.3\ (wt\%\ Mo) + 16\ (wt\%\ N) \qquad (1.24)$$

DSS-s are divided into two main groups according to PREN: duplex PREN <35 and super duplex PREN >40 [37].

In duplex steels the short crack initiation mechanism depends on the strain: at 0.8% strain the short cracks nucleate at slip marks in the austenite. On the other hand, at 1.2% strain the surface damage is almost homogeneous, but extrusions/intrusions and microcracks are located in ferrite in case of SAF 2507 [38]. In case of micronotches after one third of fatigue life, secondary cracks initiate in the ferrite phase and less frequently at the phase boundaries in case of SAF 2507 [39]. In air environment the fracture is predominantly transgranular and ductile striations exist in both phases, in artificial sea water cleavage fracture of ferrite occurs [40]. In case of high-cycle fatigue, barriers such as grain boundaries or second phases arrest the cracks or slip bands. But in case of over loading prior to reaching the fatigue limit they may overcome the barrier [41].

In [42] it was found that shrinkage cavities about 50 μm did not affect the crack propagation in cast duplex steels. It was also found that ageing tends to make fatigue fracture brittle compared to ductile fracture in un-aged condition. There is no preferential crack path between two phases but the macroscopic crack growth direction is imposed by the local crystallographic orientation of the ferrite grains.

The crack closure level is decreasing with ageing probably due to the cinematic hardening. Fatigue crack growth rates also increase by embrittlement of ferrite.

In a duplex steel 22Cr-5Ni-3Mo in case of high stress levels the crack initiation occurred mainly at persistent slip bands in the austenite or near the phase boundaries, at lower stress levels mainly at non-metallic inclusions in the surface region [1].

The corrosivity of white water depends primarily on the pH, temperature and concentration of aggressive ions. Chloride ions initiate pits, thiosulphate ions prevent passivation of an active surface and stabilize metastable pits, sulphate ions increase the conductivity of the solution, hence the environment corrosivity [32, 33].

Heat treatment of the DSS also plays a significant role, the precipitates and phase interfaces are more likely to cause pitting. The most significant negative effect on corrosion resistance and hence the corrosion fatigue is provided by the Cr-Mo-Fe rich intermetallic σ-phase [32, 42−47].

In sintered powder DSS the porosity level also decreases the corrosion resistance [48]. The corrosion resistance is further decreased by internal stresses, which can lead to increase in fatigue crack growth rate [49].

1.2 Fatigue at wear

1.2.1 Fatigue strength of wear resistant material

It is a well-known fact that there is a substantial difference between ductile and brittle materials when the weight loss in erosion is measured as a function of the impact angle. Due to their high hardness and stiffness, ceramic materials are considered to be capable of reducing scratching and micromachining type surface damage when exposed to low-angle impacting particles. At a high angle of impact, the exposed surface should be able to withstand repeated deformation. More elastic materials, such as steels, are usually preferred to cermets where cracks propagate rapidly and lead to material removal. With mixed abrasive erosive and abrasive impact wear, where a wide range of impact angles are applied, there is a controversy between material hardness and fracture toughness in the formation of wear resistance. Composite materials, especially reinforced metal-matrix composites and so called “double cemented” metal-matrix structures allow a partial solution of this problem [50].

In many wear conditions, for example sliding wear, rolling contact wear, fretting wear, the wear processes are caused by cyclic deformations [16].

High surface hardness of traditional materials does not always provide the wear resistance required for faultless operation of machine parts and tools under the conditions of erosion and impact wear. Removal of material in wear caused by impact, cyclic loading and high contact pressure occurs as a result of direct fracture or fatigue processes. Thus, toughness and fatigue properties of materials are as important as their hardness parameters.

In case of sliding induced surface fatigue, ductile materials exhibit a higher amount of subsurface crack compared to brittle materials [51].

1.2.2 Fatigue *vs*. abrasive wear resistance

If material hardness exceeds that of the abrasive, erodent particles can hardly cause plastic flow in the hard target. The degree of elastic penetration and therefore the energy transmitted to a surface depends on the elastic modulus. If it is high, less elastic penetration occurs. Therefore, as compared to abrasive hardness, the modulus of elasticity is one of the most important parameters influencing the wear resistance in the case of harder materials [52]. Under these conditions, particle impacts may cause a low-cycle fatigue failure of the reinforced metal-matrix and hard phase particles.

If the hardness of the abrasive exceeds that of the wearing material, the following processes take place: penetration of erodent particles into the material surface, microcutting or ploughing, failure of hard phase particles resulting in the detachment of small chips.

Since the erosion of brittle grains is primarily caused by a mechanism involving the initiation and propagation of microcracks, one expects that the fracture toughness of the material will influence the erosion rate. The toughness-hardness map of wear resistant materials is proposed in [53]. The wear of materials with low fracture toughness (below 10 $MPa \times m^{0.5}$ by silica erodent) is caused mainly by the brittle fracture, while the wear of materials with low hardness (less than abrasive hardness) is caused mainly by microcutting. At higher hardness and fracture toughness values, surface fatigue is dominating.

Depending on the intensity of the impact processes, the contact can lead to reversible or irreversible deformation in the surface area of the basic body. The reversible impact process generates only stresses in the target surface layer, which lie below the yield strength. Consequently, they are of elastic nature. Due to the elastic deformation, material removal can be caused by fatigue. Nevertheless, this wear component in abrasive erosion is many times lower than that caused by irreversible deformations in impact wear. The process of material removal starts after a relatively low deformation, *i.e.* at a small number of contacts between abrasive particles and the target.

Attempts to correlate the erosion rates of brittle materials with the experimental and materials parameters were made in [53, 54]. In the proposed models, hardness and fracture toughness emerge as the main material parameters that control erosion. High hardness increases the resistance to plastic deformation while high fracture toughness increases the resistance to fracture. Thus, in abrasive wear, one of the mechanisms of material removal is surface fatigue wear.

Fatigue performance of wear resistant materials under cyclic loading and at monotonic loads has been studied by different researchers [17, 55]. It has been found that the adhesive wear fracture and fatigue start similarly – predominantly in the binder phase (extrusion-intrusion mechanism), in contrast to abrasive erosion and sliding wear [55].

1.3 Conclusions to the chapter

1. As regards duplex stainless steels:

As it follows from the literature overview the process of corrosion fatigue in case of duplex stainless steels is quite complicated. Mainly it depends on the microstruture (heat treatment), the loading scheme, temperature, application and chemical composition of the corrosive environment. Usually fatigue data are obtained using rotating bending scheme where the corrosive media is sprayed onto the specimen. This leads to a situation where the corrosive media is aerated. The oxygen introduced favours the oxidation of the specimen surface. The effect of corrosion and the microstructure has been discussed in the literature. Heat treatment of DSS leads to higher corrosion resistance but on the other hand introduces residual stresses, which have a negative effect on fatigue performance. Therefore it is of interest studying the corrosion fatigue of PM DSS in HIP-ed condition in case of axial loading and specimen immersed into corrosive media. Also to compare fatigue performance of DSS at different mean stress levels. The overview also showed that the corrosion fatigue of duplex steels in as cast condition is not widely available. The data for direct comparison of fatigue properties of PM duplex stainless steel in air and in corrosive environment are not available.

2. As regards wear resistant materials:

The estimation of the fatigue strength of wear resistant materials, particularly powder metallurgical (PM) materials, being mainly composite materials and containing pores, defects or inhomogeneities is important both from the theoretical and practical point of view. These materials are classified as so-called "structurally brittle" materials and their behaviour at different wear conditions may be unpredictable.

The main probable mechanisms at abrasive erosion and impact wear of PM produced wear resistant materials are microcutting and low-cycle fatigue, but data about the fatigue of wear resistant materials practically missed and the role of fatigue at wear is not widely studied.

1.4 Aims of the study

1. The study of the corrosion fatigue behaviour of powder duplex stainless steel at tension /compression:

- to clarify the possibility of predicting fatigue strength in corrosive environment;
- to clarify the influence of synthetic white water environment by direct comparison of fatigue properties in air and in synthetic white water environment,
- to clarify the influence of synthetic white water environment along with mean stress.

2. Study of the surface fatigue behaviour of powder steels at contact fatigue:
- to clarify the role of fatigue processes of powder steels at abrasive erosion and impact wear;
- to find a correlation between surface fatigue and wear resistance.

To achieve the above mentioned aims the following activities were planned:
- a study of corrosion fatigue at tension/compression of duplex stainless steels to determine the fatigue strength;
- a study of the fracture mechanism at corrosion fatigue;
- a study of abrasive erosion and impact wear resistance of powder steels;
- a study of surface fatigue wear of powder steels;
- a study of the wear mechanism at surface fatigue wear and estimate its role in wear.

2 EXPERIMENTAL

2.1 Materials to be tested

2.1.1 Duplex stainless steels

The specimens included in corrosion fatigue testing were:
- produced by powder metallurgy (PM) and Hot Isostatic Pressing (HIP) duplex stainless steel (DSS);
- cast and hot rolled DSS;
- super duplex stainless steels (SDSS) in as-cast condition.

An overview of the tested DSS-s is given in Table 2.1. Steels Duplok22 and 3Re60 were compared to each other, Grade 5A was only used as a reference material.

Table 2.1 Overview of the tested steels

Grade	Type	Condition	Number of specimens
Duplok22	Duplex	PM-HIP-ed	35
3Re60	Duplex	Cast/hot rolled	14
Grade 5A	Super Duplex	As-cast	11

Tested steels Duplok22 and 3RE60 are low-alloy DSS-s. Duplok22 is fully dense HIP-ed PM DSS. HIP process that was used to compact and densify the initial powder was carried out for four hours at 1140 °C and 100 MPa, after which the specimens were slowly cooled along along the furnace. Steel 3Re60 is cast and subsequently hot rolled DSS. Hot rolling is used in order to make the microstructure finer and more homogeneous compared to as-cast state.
According to ASTM A-890-99a, steel Grade 5A is a SDSS that is in an as-cast condition. It is similar to the commonly used forged steel SAF2507 in its chemical

composition. This SDSS was only used for comparing the corrosion fatigue properties at symmetrical loading.

Chemical composition

In order to evaluate the pitting resistance of DSS a chemical analysis was made using Spectrolab M for atomic emission by the spark method.

According to the PRE number, the highest pitting resistance was in case of Grade 5A, the lowest 3Re60 and the medium for Duplok22 (~42, ~29 and ~34 respectively). The chemical composition of the tested materials is shown in Table 2.2. In order to further distinguish the main phases found, the chemical composition of the ferrite and austenite phases was also determined by means of an EDS analysis using SEM equipped with EDS capability (Table 2.3). In a qualitative SEM, a line scan was made to determine the distribution of the chemical elements in two main phases (Fig. 2.1). It appears that the chemical composition of the phases is quite homogeneous and there seems to be no noteworthy accumulation of chemical elements onto the interphase borders.

Table 2.2 Chemical compositions of the tested steels (the average of at least three measurements), wt%

Grade	**C**	**Si**	**Mn**	**P**	**S**	**Cr**	**Mo**	**Ni**	**Al**	**N**
Duplok22	0.02	0.59	1.20	0.02	0.001	21.09	2.74	5.56	0.01	-
3Re60	0.02	1.44	1.48	0.08	0.021	18.29	2.46	5.14	0.01	-
Grade 5A	0.03	0.48	0.80	0.03	0.008	23.48	3.69	8.11	0.02	-
Uncertainty *U*(*k* =2)	±0.01	±0.13	±0.28	±0.01	±0.005	±0.98	±0.40	±0.50	±0.01	-

Table 2.3 Chemical compositions of the ferrite (α) and austenite (γ) (the average of at least three measurements), wt%

Grade	**Phase**	**Si**	**Cr**	**Mo**	**Mn**	**Ni**
Duplok22	***α***	0.69	22.75	3.75	1.08	3.23
	γ	0.56	20.31	2.67	1.37	6.03
3Re60	***α***	1.58	19.50	3.64	1.23	3.56
	γ	1.28	16.94	2.21	1.59	5.76
Grade 5A	***α***	0.42	25.50	5.28	0.69	6.05
	γ	0.48	22.14	3.28	0.85	9.49
Uncertainty *U*(*k*=2)		±0.12	±1.02	±0.44	±0.25	±0.52

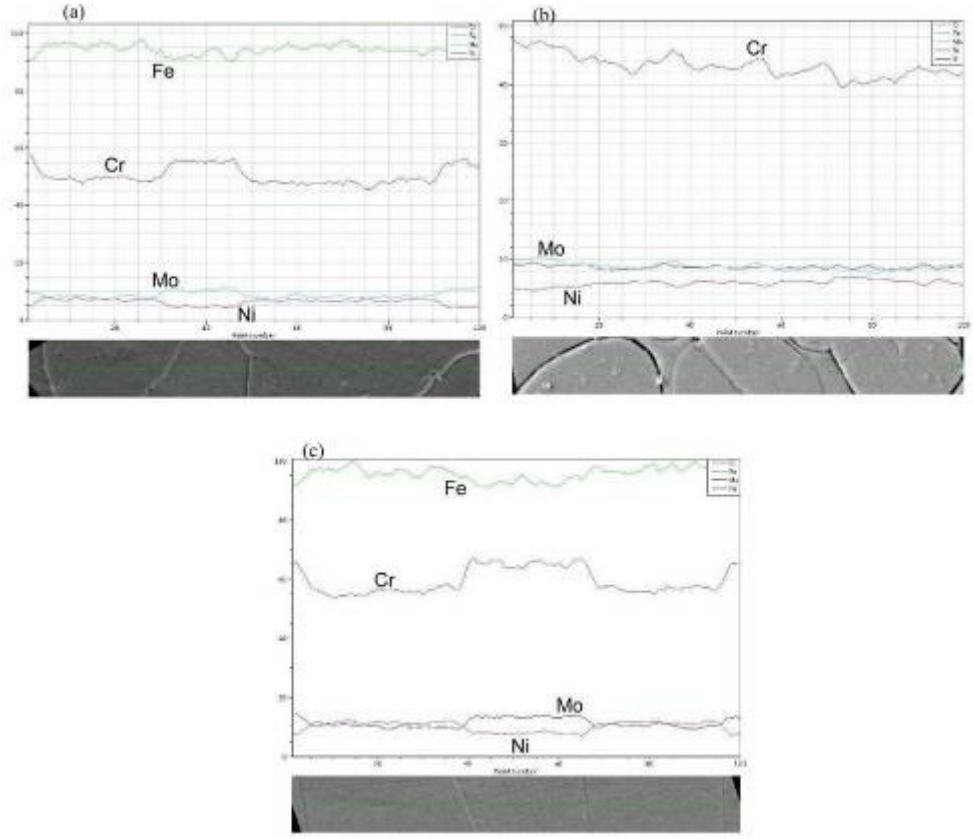

Figure 2.1 Distribution of chemical elements in ferrite/austenite phases: a – Duplok22; b – 3Re60; c – Grade 5A (SEM, EDS)

Microstructures of tested DSS-s

In order to reveal the microstructures of tested DSS-s for further analysis, electrochemical etching using NaOH water solution (40g NaOH and 100ml distilled water) was used. The etching was carried out during 2 – 5 seconds and at 2–3 Volts. After etching, samples were rinsed in ethanol and dried in the air. This type of etching makes ferrite dark and also reveals other phases found in the microstructure, such as intergranular austenite (γ_i) and σ-phase.

Microstructures of DSS-s are given in Figs. 2.2–2.4 in parallel and perpendicular direction to the axis of the specimen. In all the DSS-s, the microstructure consists of austenite "islands" in the ferrite matrix. In Fig. 2.2 the microstructure of PM HIP Duplok22 can be seen. Compared to steels 3RE60 and Grade 5A it has a fine and homogeneous microstructure. There is no visible intergranular austenite or σ-phase, only some occasional very small non-metallic inclusions. The largest single non-metallic inclusion was found to be about 663 μm^2.

Table 2.4 Amount of ferrite (*α*) and austenite (*γ*) along (AA) and perpendicular to the axis of the specimen (PA) in the tested steels (the average of at least three measurements), vol%

Grade	**Direction**	**Ferrite phase (*α*)**	**Austenite phase (*γ*)**
Duplok22	AA	73	27
	PA	62	38
3Re60	AA	66	34
	PA	66	34
Grade 5A	AA	51	49
	PA	57	43
Uncertainty *U*(*k*=2)		±10	±10

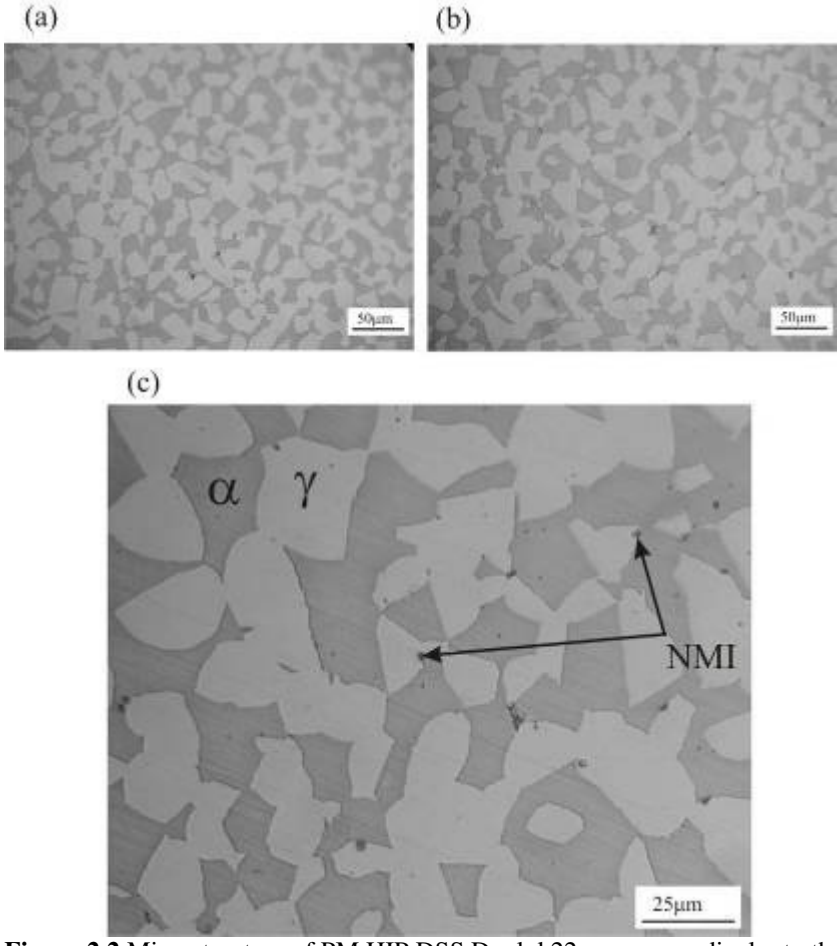

Figure 2.2 Microstructure of PM HIP DSS Duplok22: a – perpendicular to the axis; b – along the axis; c – at higher magnification (α – ferrite, γ – austenite, NMI – non-metallic inclusions) (LOM)

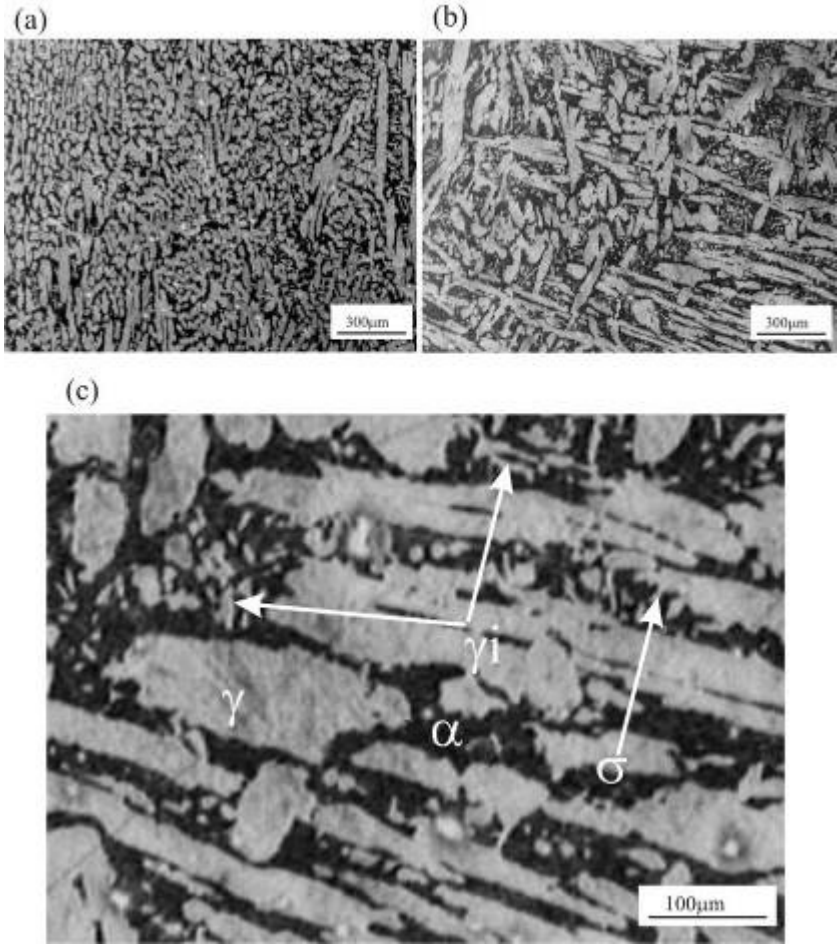

Figure 2.3 Microstructure of DSS 3RE60: a – perpendicular to the axis; b – along the axis; c – at higher magnification (α – ferrite, γ – austenite, σ – sigma phase) (LOM)

The steel 3Re60 has a different microstructure along and perpendicular to the specimen axis as can be seen on Fig. 2.3. The hot rolling direction can be seen, to some extent the microstructure has re-crystallized during hot rolling. The SDSS Grade 5A had a similar microstructure along and perpendicular to the axis of the specimen (Fig 2.4).

The volume fraction of ferrite (α) and austenite (γ) is given in Table 2.4. The results were obtained by analysing the photos taken by LOM from electrochemically-etched micrographs using Buehler's Omnimet image analysis system.

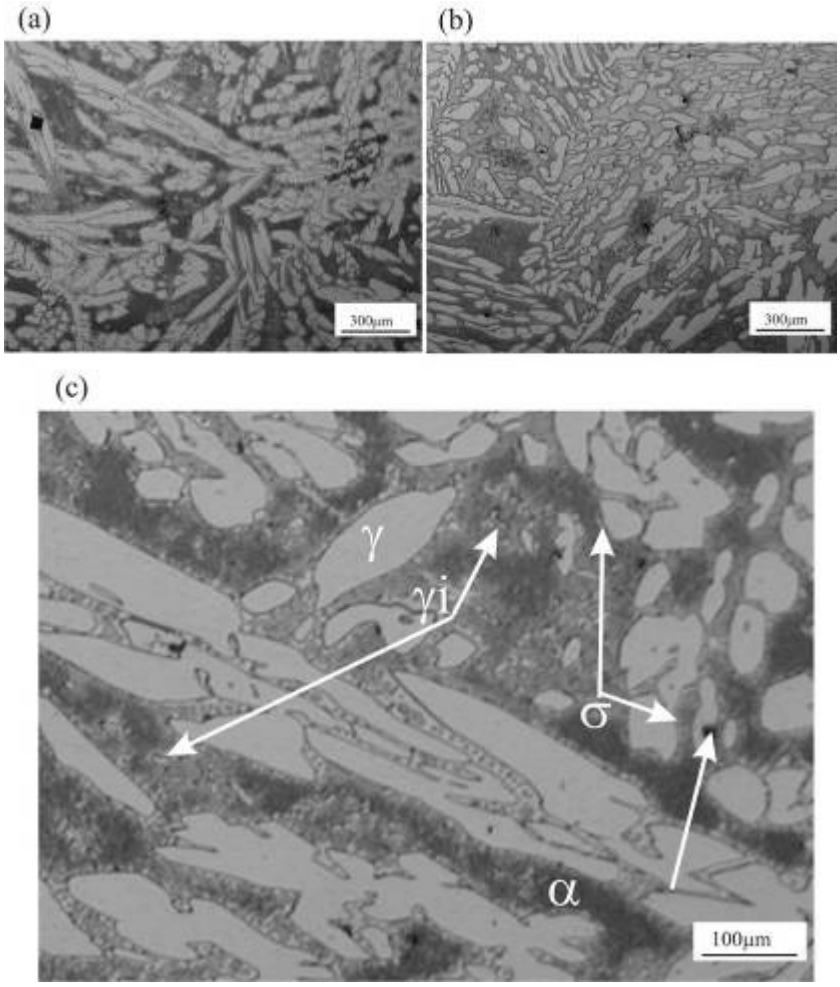

Figure 2.4 Microstructure of SDSS Grade 5A: a – perpendicular to the axis; b – along the axis; c – at higher magnification (α – ferrite, γ – austenite, NMI – non-metallic inclusion, σ – sigma phase) (LOM)

Tensile properties of tested DSS-s

The mechanical properties were determined in order to predict the fatigue performance of powder DSS and compare the tested DSS-s (Table 2.5).

The results were obtained using Instron 8516 type 100 kN servo-hydraulic test machine and an extensometer. Testing was carried using round specimens, manufactured from the grip ends of the corrosion fatigue tested specimens, along the axis according to the EVS-EN 10002-1 [56].

Table 2.5 Tensile properties of tested DSS-s along the axis of the specimen (the average of three measurements)

Grade	**Tensile strength R_m (S_u), MPa**	**Proof strength $R_{p0.2}$, MPa**	**R_m /$R_{p0.2}$**
Duplok22	832	529	1.57
3Re60	766	491	1.56
Grade 5A	700	528	1.32
Uncertainty $U(k=2)$	±17	±12	-

Hardness of the tested steels was measured according to EVS-EN ISO 6507-1:2006 [57] using 98 N (10 kgf) load and Vickers hardness testing machine Indentec 5030 SKV. The results are given in Table 2.6. It appears that the HV10 hardness of the tested DSS is quite the same.

Table 2.6 HV10 hardness of the tested DSS-s (the average of three measurements)

Grade	**Perpendicular the axis**	**Along the axis**
Duplok22	234	236
3Re60	248	234
Grade 5A	234	235
Uncertainty $U(k=2)$	±12	±12

For microhardness measurements, the Buehler Micromet 2001 microhardness tester was used. The results are given in Table 2.7. As follows from Tables 2.6, the HV10 hardness was about the same for all the tested steels. However, noticeable deviation in microhardness of the constituent phases along and perpendicular to the axis was observed in case of Duplok22 (Table 2.7). According to the results, austenite is the harder phase. It means ferrite is more likely to deform during loading. This was confirmed by analysing the photo taken from single point indentation test where fatigue striations were seen mostly in ferrite.

Table 2.7 HV0.01 hardness of the tested DSS-s ferrite (α) / austenite (γ) phases along the axis (AA) and perpendicular to the axis of the specimen (PA) (the average of at least three measurements)

Grade	**Direction**	**Ferrite (α)**	**Austenite (γ)**
Duplok22	AA	276	300
	PA	321	369
3Re60	AA	266	277
	PA	286	286
Grade 5A	AA	301	328
	PA	296	327
Uncertainty $U(k=2)$		±24	±24

Uncertainty calculations
The uncertainty (u) of the results was calculated as follows [58]:

$$u = \sqrt{u_1^2 + u_2^2}\text{, where} \quad (2.1)$$

$$u_1 = \frac{x_{\max} - x_{\min}}{2\sqrt{3}}\text{, and} \quad (2.2)$$

$x_{\min}$ – is the minimum value of the obtained measurement;
$x_{\max}$ – maximum value of the obtained measurement;
u_2 – uncertainty due the testing machine.

The overall uncertainty (U) at confidence level k = 2 (95%) was calculated as follows:

$$U(k{=}2) = k \times u. \quad (2.3)$$

2.1.2 Wear resistant materials

The materials studied include PM produced materials (Table 2.8) and conventional steels as reference materials. These materials are commonly used in many applications where resistance to abrasive erosive wear or impact wear is required. The microstructure, obtained by SEM analysis, of powder materials is presented in Fig. 2.5.

Table 2.8 Microstructure and hardness of the studied materials

Material	**Microstructure**	**Density, kg/m^3**	**Hardness HV**
Powder materials MMC Weartec	 PM/HIP-ed (Cr-steel + VC) + WC; reinforcements: ~20 vol% VC (d ~1μm) and ~20 vol% WC (200 – 300 μm); SF/HIP-ed high speed steel (HSS), fine-grained	 9900 7300	 550/1540 HV10 (1074 HV50) 816 HV10
Conventional steels Hadfield steel Hardox 400	 Austenite Martensite+troostite	 7800 7800	 217 HV10 303 HV10

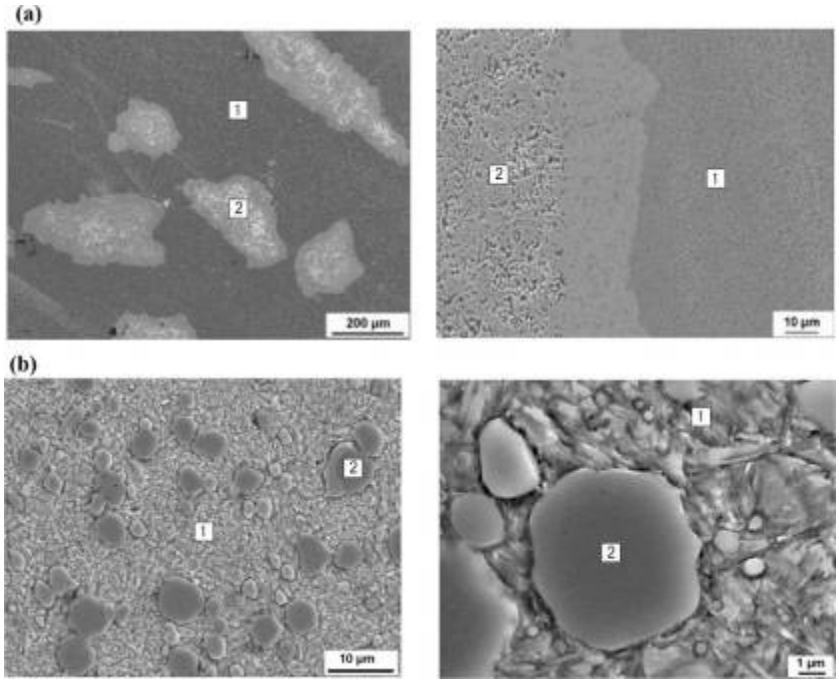

Figure 2.5 Microstructure of the studied powder materials: a – MMC (1 – Cr-steel with VC; 2 – WC); b – Weartec (1 – Cr-Mo-V-steel; 2 – VC) at different magnifications (SEM)

2.2 Test methods

2.2.1 Corrosion fatigue testing

In order to obtain the corrosion fatigue data for the DSS-s axial tension-compression method was used. The load-controlled testing was carried out at 15 Hz frequency using a Instron 8516 type 100 kN servo-hydraulic test machine. The specimens were partially submerged in the test environment in a test chamber (Fig. 2.6). A membrane pump was used to circulate the test solution (3 l) about twice an hour (test chamber volume about 0.7 l). The test chamber was made of stainless steel and coated with Teflon. The test end criterion was failure of the specimen at any given stress level or reaching 10^7 cycles (run-out).

The test variable was the alternating stress level S_{alt}, and output cycles count. The S_{alt} values were chosen to cover the S-N curve from 10^4 to run out (10^7) cycles. The test parameters are given in Table 2.9.

The round specimens were ∅ 10 mm at the grips, ∅6 mm at the 24 mm long test section and 170 mm in total length (Fig. 2.7).

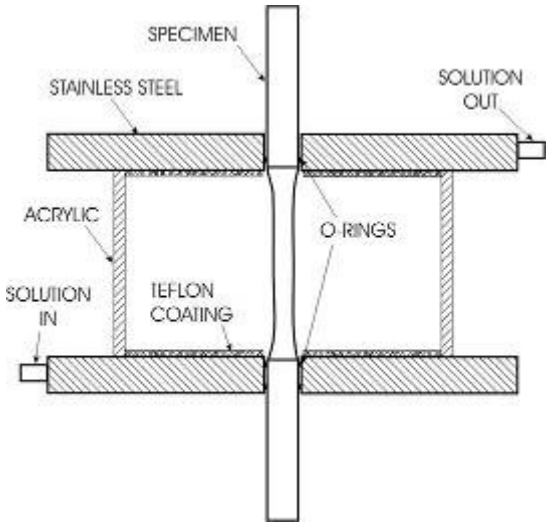

Figure 2.6 Test cell used for submerging the specimen into the corrosive environment

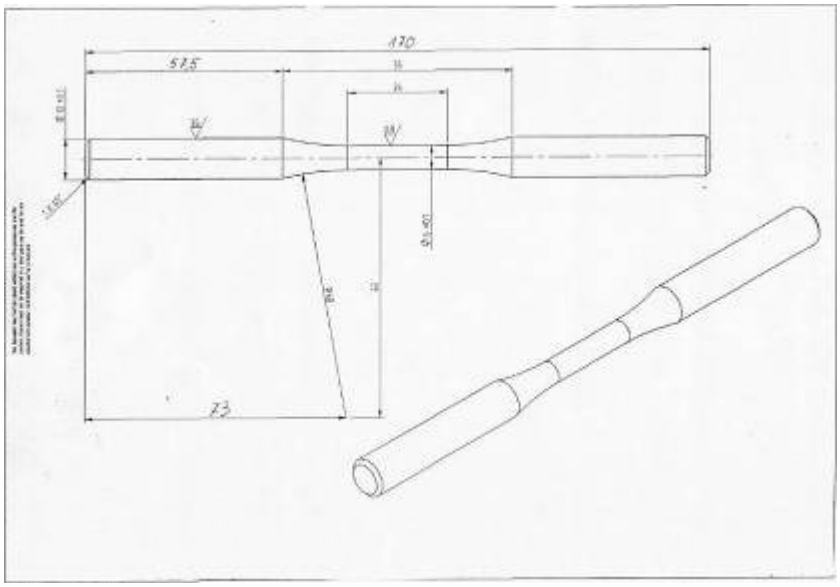

Figure 2.7 Drawing of a round specimen used in corrosion fatigue testing

Table 2.9 Corrosion fatigue testing parameters of studied steels

Grade	**Type**	**Condition**	**Testing frequency, Hz**	**Mean stress, MPa**	**Number of specimens**
3Re60	Duplex	Cast/hot rolled	15	0, 70, 121	14
Duplok22	Duplex	PM-HIP-ed	15	0, 70, 126	35
Grade 5A	Super Duplex	As-cast	15	0	11

In order to reduce the scattering of the test results by premature failure due to the crack initiation from the machined specimen surface all the specimens were polished. The specimens were mechanically polished at the test section and blending fillets to remove scratches, using a polishing wheel and abrasive. The routine for the specimen preparation was is given elsewhere (Paper II).

The required surface roughness Ra was <0.6 µm and it was measured by the stationary surface measurement device MAHR Concept. The effect of surface roughness on fatigue was not studied.

The testing environment was a modified using Sandusky's new solution containing chloride (Cl^{-1}), sulphate (SO_4^{2-}) and thiosulphate ($S_2O_3^{2-}$) ions dissolved in distilled water and the pH of the test solution was adjusted to 3.5 by adding 1vol% H_2SO_4.

Composition of the test solution is shown below (prior to pH adjustment):

- (NaCl), Cl^{-1} – 1000 ppm;
- ($Al_2(SO_4)3\times18H_2O$), SO_4^{2-} – 800 ppm;
- ($Na_2S_2O_3\times5H_2O$), $S_2O_3^{2-}$ – 200 ppm.

This ion ratio of 20 (Eq. (2.4)) was chosen according to the in order to cause maximum pitting corrosion [57]:

$$(Al_2(SO_4) + NaCl)/Na_2S_2O_3 = 10 – 20. \quad (2.4)$$

Above this range, there is insufficient thiosulphate to reach the pit nucleous. Below this range, there is too much thiosulphate reduction to bisulphate, which would prevent the acidification of the pit required for further growth [5].

The pH was monitored daily and the expiration time for a solution was three days. During testing the pH value increased about 0.1 units per 24 hours.

Fatigue testing in air

Fatigue testing in the air was carried out to compare the results with those of corrosion fatigue testing in case of Duplok22 in order to evaluate the effect of the synthetic white water environment on the fatigue performance.

Testing in the air was carried out using the same Instron 8516 test machine that was used for corrosion fatigue testing. The specimens round Ø 10 mm at the grips, Ø 5 mm at the 10 mm long parallel part and 50 mm in total length were manufactured by turning the corrosion fatigue specimens from the grips.

2.2.2 Surface fatigue testing

In order to quantify surface fatigue wear (SFW), a test system, which produces repeated stresses on the material surface, was used (Fig. 2.8) [17]. It consists of a servo-hydraulic test machine Instron 8800, an indentor, a special specimen holder, and a base plate. The indentor was a hardmetal cone with tip angle of 120º and radius of 350 µm and was replaced at the start of a new series of test. The test procedure was as follows: after each indentation, the specimen was moved by a distance of 400 µm to cover an area of 6×6 mm with a regular rectangular pattern. 30 000 cycles with a normal load of 1500 N were used to produce surface fatigue

wear in the studied materials. The surface fatigue wear was characterized by mass loss of each tested sample. To study the wear mechanism at surface fatigue a single point loading with normal load of 1500 N was also investigated. An air blower was used to remove the debris from the surface during testing.

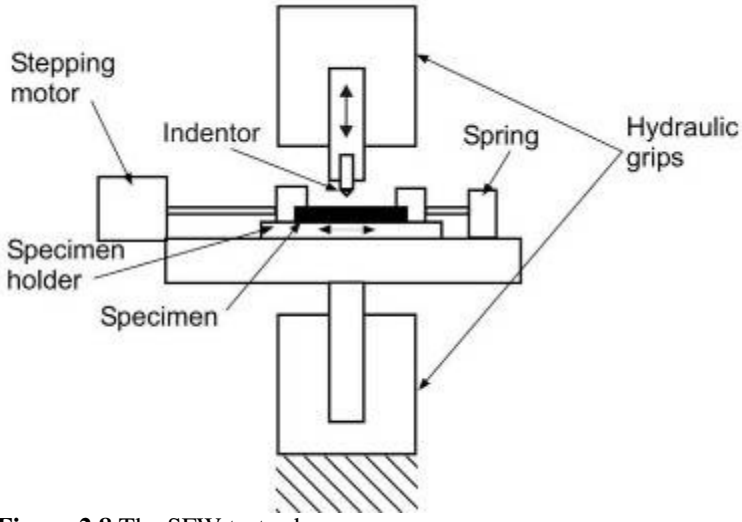

Figure 2.8 The SFW test scheme

2.2.3 Abrasive wear testing

Abrasive erosive wear

Abrasive erosive wear (AEW) was determined with the centrifugal accelerator CAK-5 (Fig. 2.9) at the velocity of 80 m/s and impact angle of 90º with quartz sand (0.1 – 0.3 mm). The specimens are attached to the stationary outer ring where their surfaces are eroded by the erodent particles accelerated by the centrifugal force from the rotor. The wear is characterized by mass loss of each tested sample and the volumetric wear rate I_v in mm^3/kg and relative wear resistance ε_v were calculated.

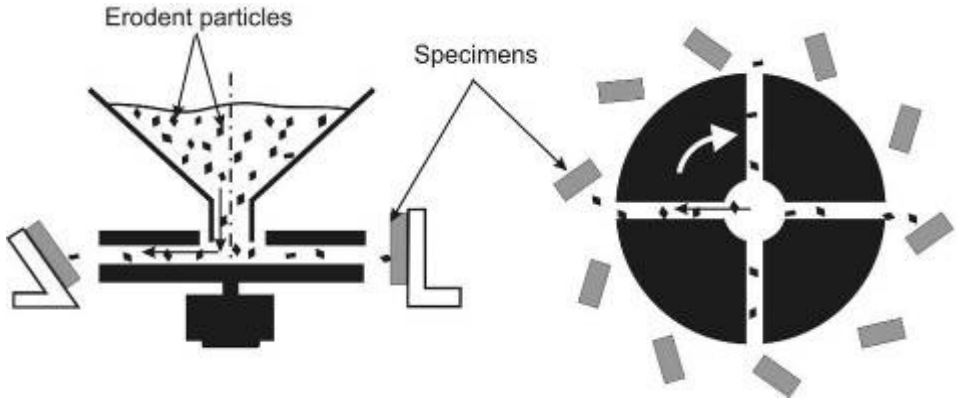

Figure 2.9 Schematic presentation of a centrifugal accelerator used for abrasive erosive wear testing

Abrasive impact wear

Abrasive impact wear (AIW) resistance of materials was determined by an experimental disintegrator based impact tester DESI (Fig. 2.10) at the erodent linear velocity of about 60 m/s and an impact angle of about 90º. As abrasive granite gravel (4 – 5.6 mm) was used. The specimens were attached to the crushing fingers of the single rotor used. The wear was characterized by mass loss of each tested sample. The volumetric wear rate I_v in mm^3/kg and the relative wear resistance ε_v were calculated similar to AEW.

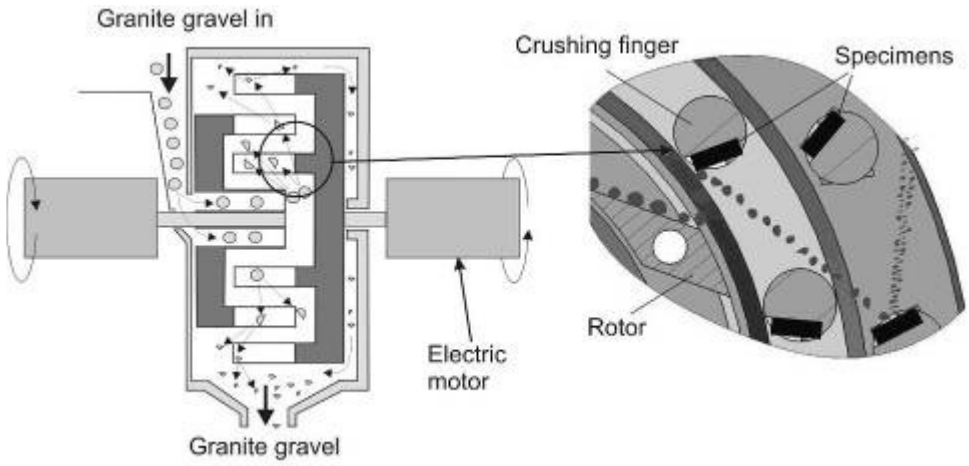

Figure 2.10 Schematic presentation of experimental disintegrator-based impact wear tester DESI used for impact testing

2.2.4 Fractography and topography studies

In order to investigate the fracture surfaces of the tested fatigue specimen in case of DSS-s, as well as the worn surfaces after wear tests of wear resistant materials,

both light optical microscope (LOM) and scanning electron microscope (SEM) JEOL-840A and Hitachi TM1000 analysis were made. Samples were examined starting from low magnifications (5× in case of LOM, 20× in case of SEM) up to about 1000× in case of SEM, in order to reveal the characteristic aspects of the examined surfaces. In case of DSS-s, the main focus was on three distinct zones of fracture surfaces (Fig. 2.11).

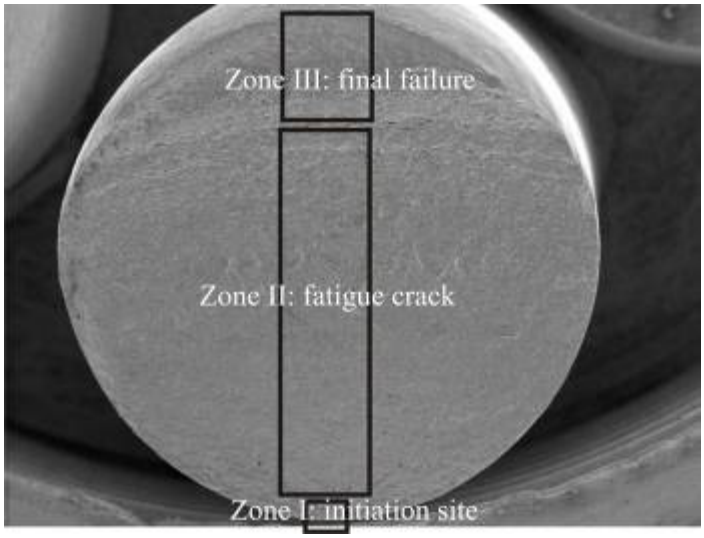

Figure 2.11 The zones investigated by SEM in DSS fractography analysis

3 RESULTS AND DISCUSSION

3.1 Corrosion fatigue testing

Based on environment assisted fatigue tests fatigue strengths of studied steels were determined. Log S_{alt} – log N curve was chosen for data presentation. First goal was to analyse the test data for R = –1 by the means of MS Excel. It was seen that a straight line could approximate the data. Hence linear regression routine could be employed to estimate the fatigue strength coefficient S'_f and fatigue strength exponent b (Eq. (1.8)). The results are obtained using linear regression routine and Eq. (1.8) are presented in Table 3.1.

Table 3.1 The results of linear regression analysis (calculated fatigue coefficients)

Grade	**S'_f, MPa**	***b***
Duplok22	699	–0.041
Duplok22air	565	–0.024
3Re60	711	–0.052
Grade 5A	1036	–0.106

The actual (measured) data obtained by testing along with calculated S_{alt} and formulas are given in Fig 3.1. Good agreement could be seen, Eq. (1.8) can be applied for the current test setup and

materials. The fatigue strength obtained by linear regression routine are referred to as "calculated" results.
There are limitations to the predicted S-N curve [6]: only valid for the presented test data, test scheme and environment; representative of the median fatigue data; log-normal distribution of *N* is assumed.

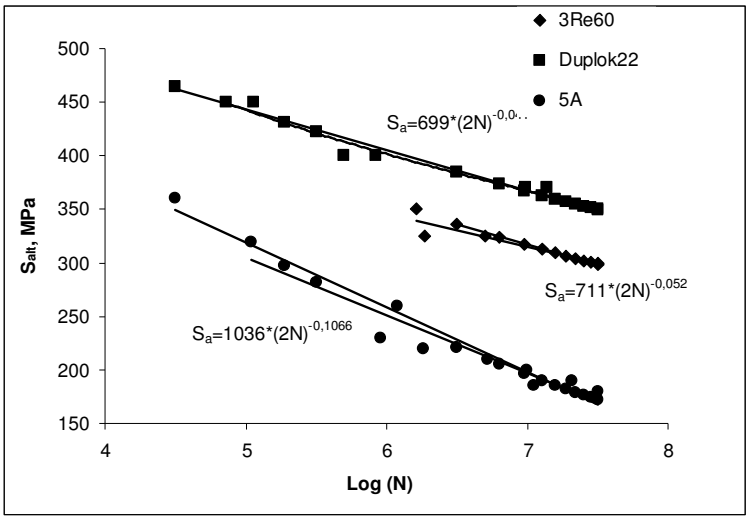

Figure 3.1 S-N curves: measured and calculated fatigue performance for steels Duplok22, 3Re60 and Grade 5A (R = –1)

The test results also comply with the tensile properties shown in Table 2.5. Steel Duplok22 with the highest tensile strength had the highest corrosion fatigue strength.

Comparison of corrosion fatigue strength and fatigue limit of Duplok22
In the current study, neither the effect of different corrosive environments nor the effect of loading frequency was studied. But as it follows from literature, these two factors are important. When comparing the obtained corrosion fatigue strength Duplok22 with a specification of similar material [59] where the fatigue is 275 MPa (at 10^9 cycles) it appears that they are quite different. The result presented in the literature is obtained in a less corrosive test solution containing 100 ppm Cl^{-1}, 1000 ppm SO_4^{2-} ions and at pH 3.5 (TIP 0402-09 type I) by rotating bending and in addition to that the testing frequency is unknown.

In case of steel 3Re60 the fatigue strength is higher when comparing the material specification [60] 200 MPa at 5Hz and 265 MPa obtained at 25 Hz. The literature results were obtained by rotating bending in a test solution containing 400 ppm Cl^{-1}, 250 ppm SO_4^{2-} ions and at pH 3.5.

In order to evaluate the effect of corrosive environment on fatigue performance of PM HIP Duplok22, fatigue testing in air was carried out. The test data was analysed the same way as described earlier and the fatigue limit was 390 MPa. This

is higher than the corrosion fatigue strength at the same cycle level (350 MPa) (Fig. 3.2). The difference in results could be probably explained by studying the effect of corrosive environment in detail in a future research.

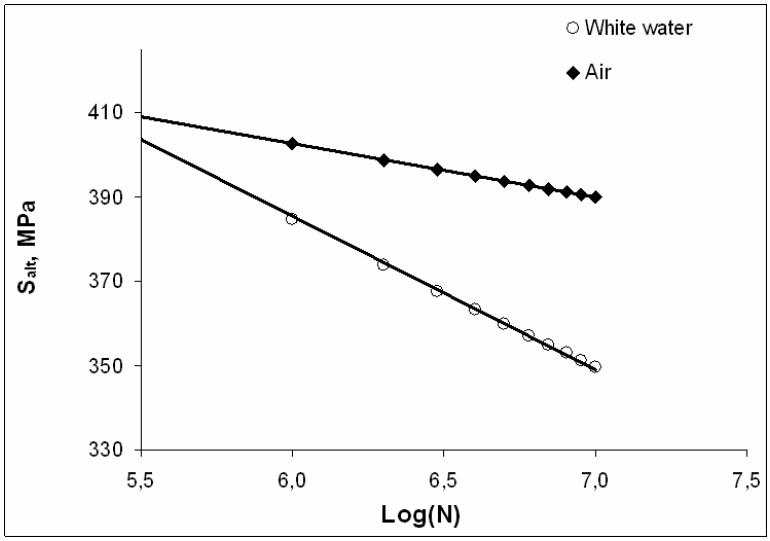

Figure 3.2 S-N curves: fatigue performance of Duplok22 in air and in corrosive environment

Corrosive environment starts to influence the results quite early, after about 10^6 cycles. This means in about 24 hours when the testing frequency is 15 Hz. This is probably due to the fact that corrosion has very little time to act in lower cycles, and in case of higher testing frequencies the effect of corrosion appears in much later stages.

Prediction of corrosion fatigue strength (S_{1000}) *at* 10^3 *cycles*

In order to plan the fatigue testing in addition to prediction of the fatigue limit fatigue strength at 10^3 cycles should be estimated. The fatigue strengths predicted are referred to as "predicted" results. According to Fig. 3.3, corrosion does not have enough time to influence the results in low-cycle fatigue area, hence the results should be estimated in the usual way. An example of that is Eq. (1.2) ($S_{1000,\ R} = S_{1000} \times C_R$), which is based on the tensile strength of a material. Since there was no data for 10^3 cycles MS Excel based analysis was used for calculating fatigue strength at 10^3 cycles.

It can be seen that Eq. (1.2) does not suit the test results exactly (Table 3.2).

Although HV hardness measurements are easiest to conduct, the best solution could be using more reliable tensile strength as a basis for calculating the S_{1000}, especially when taking into account that HV10 values of the tested materials were virtually the same. According to our study and tested steels, tensile strength based prediction works the best, S_{1000} is about $(0.61 - 0.65) \times S_u$.

Table 3.2 Calculated corrosion fatigue strength (S_{1000}), calculated and predicted fatigue ratios at 10^3 cycles (R = −1)

Grade	Calculated					Predicted
	S_{1000}, MPa	S_u, MPa	HV	S_{1000} / S_u	S_{1000} / HV	S_{1000} / S_u (Eq. (1.2))
Duplok22	511	832	236	0.61	2.17	0.75
3Re60	472	766	234	0.61	2.01	
Grade 5A	461	700	235	0.65	1.96	

Prediction of corrosion fatigue strength (S_f) *at* 10^6 and 10^7 cycles

The equations (1.3) and (1.4) are for prediction of base line fatigue strength (S_{be}) of small and polished bending samples at 10^6 cycles in non-corrosive environment. However, the attempt to predict the fatigue strength at 10^6 cycles by these equations showed that they did not predict the fatigue strength accurately for all the tested DSS. The tensile strength based calculation (Eq. (1.3)) allowed predicting the S_f at 10^6 cycles quite well when the loading factor C_L = 0.9 was used (Table 3.3).

Table 3.3 Measured fatigue strength (S_f) (MPa), measured and predicted fatigue ratios of tested DSS-s at 10^6 cycles (R = −1)

Grade	Measured			Predicted			
	S_f	S_f / S_u	S_f / HV	S_f / S_u, C_L=0.75 Eq. (1.3)	S_f / S_u, C_L=0. 90 Eq. (1.3)	S_f / S_u, C_L=0.75 Eq. (1.4)	S_f / S_u, C_L=0.90 Eq. (1.4)
Duplok22	385	0.46	1.64	0.38	0.45	0.25	0.3
3Re60	331	0.43	1.41				
Grade 5A	221	0.32	0.94				

When considering the hardness of a material for estimating the corrosion fatigue strength at 10^7 cycles of tested DSS (Eq. (1.7)), the best fit can be found only in case of Duplok22 when the corrosion fatigue strength was in compliance with the lower bound value obtained (Table 3.4). This equation is meant to be used for material free of major defects, and it appears that the fine and homogeneous microstructure of PM produced Duplok22 suits that need. Tensile strength based analysis could only be used for predicting fatigue strength at 10^7 cycles when tolerance field is applied:

$$S_f = (0.3 \pm 0.05) \times S_u. \quad (3.1)$$

Table 3.4 Measured corrosion fatigue strength (S_f) (MPa), measured and predicted fatigue ratios of tested DSS-s at 10^7 cycles (R = −1)

Grade	Measured			Predicted
	S_f	S_f / S_u	S_f / HV	S_f / HV Eq. (1.7)
Duplok22	350	0.42	1.50	1.6 ± 0.1
3Re60	300	0.33	1.30	
Grade 5A	175	0.26	0.74	

It seems that the available calculations do not adequately describe the tested DSS with some exceptions in case of Duplok22 and 3Re60. This implies that corrosion fatigue prediction needs to be dealt case-by-case taking into account the corrosive environment, testing frequency and loading scheme.

Mean stress effect

The mean stress effect is expressed as a S_{alt} – log N curve plot with alternating stress *vs.* cycle number. The data analysis was done as described earlier.

The previously calculated and predicted coefficients are shown in Table 3.5. Difference can be seen which, means that the curves plotted using these coefficients do not represent the actual test data as can be seen in Fig 3.3 when using Eq. (1.11).

Table 3.5 Linear regression results: calculated coefficients in case of mean stresses

Grade	S_m, MPa	Calculated		Predicted	
		S'_f, MPa	b	S'_f, MPa	b
Duplok22	70	974	–0.068	630	–0.041
	126	906	–0.063	574	–0.041
3Re60	70	941	–0.075	641	–0.051
	121	995	–0.088	590	–0.051

It can be seen from Fig. 3.3 that increase in mean stress S_m at some fatigue life (cycles) is followed by decrease in alternating stress S_{alt} (Table 3.6).

Mathematically this is expressed by Eqs. (1.18 – 1.20) or Eq. (1.11). In addition the SWT (Smith, Watson and Topper) equation (3.2) can be used [6]:

$$S_{cr} = \sqrt{S_{\max} \times S_{alt}}\ , \qquad (3.2)$$

where: $S_{max} > 0$; S_{cr} – fully reversed stress amplitude for a given fatigue life (cycles). In case of fatigue limit (10^7) the $S_{cr} = S_e$.

This can also be observed in the calculated (Eqs. (1.18 – 1.20)) "fail safe" stress levels for the run-out cycle count (10^7) which appear to be greater compared to those actually obtained from the testing (Table 3.6).

Table 3.6 Comparison of measured and predicted S_{alt} at 10^7 cycles, MPa

Grade	Measured				Predicted				
	S_m	S_{max}	S_{min}	S_{alt}	Good-man model	Soder-berg model	Gerber model	SWT model	Eq. (1.11)
Duplok22	0	350	–350	350	350	350	350	350	350
Duplok22	70	350	–210	280	321	304	344	321	315
Duplok22	126	425	–173	299	297	267	330	327	287
3Re60	0	300	–300	300	300	300	300	300	297
3Re60	70	320	–180	250	273	257	294	280	268
3Re60	121	320	–78	199	253	226	282	252	246

When comparing the S_{alt} values at 10^7 cycles to the corresponding calculated values some differences can bee seen. In case of symmetrical loading, the calculated cycle counts are equal to the actual fatigue limit of the material.

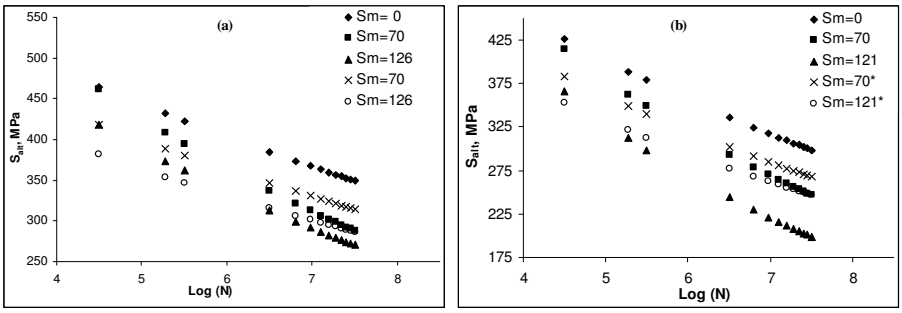

Figure 3.3 Mean stress effect on fatigue strength: a – of Duplok22; b – 3Re60
(* predicted values)

Figure 3.4 shows the predicted S_{cr} *vs*. actual S_{cr} at 10^7 cycles, once again it is shown that the models are not able to fully predict the S_{cr} values. In case of Duplok22 at S_m = 0 and 126 MPa, only the Goodman model seems to be the best fit. How ever in case of S_m = 70 MPa, the test results are lower than predicted by Goodman, this is probably due to the effect of inclusions. In case of 3Re60, the actual results are lower than those predicted. It seems that the tensile mean stresses lower the material ability to withstand loading more than predicted, but the effect is more uniform than in case of PM Duplok22. This is probably due to the microstructure, which is not as homogeneous as Duplok22, and the effect of inclusions is less obvious.

An attempt to combine the Eqs. (1.7) and (1.16) produced the following results:

$$\sigma_w = [1.6\ \text{HV} \pm 0.1\ \text{HV}]\ [(1 - R)/2]^{\alpha}. \qquad (3.3)$$

The predicted fatigue strength at 10^7 cycles for Duplok22 in case of mean stresses is shown in Table 3.7 (Eq. 1.16).

Table 3.7 Measured and predicted fatigue strength at 10^7 cycles σ_w for Duplok22 in case of mean stress, MPa

	Measured		**Predicted**	
S_m	70	126	70	126
σ_w	280	299	332 – 354	322 – 343

It can be seen that the results overestimated the actual results. Over all the described methods for evaluation of the mean stress they only seem to partially apply to corrosion fatigue. The best method to be used therefore would be the Eq. (1.11) and corrected fatigue coefficients based on measured fatigue data. The predictions apply to the tested samples, test environment and loading scheme.

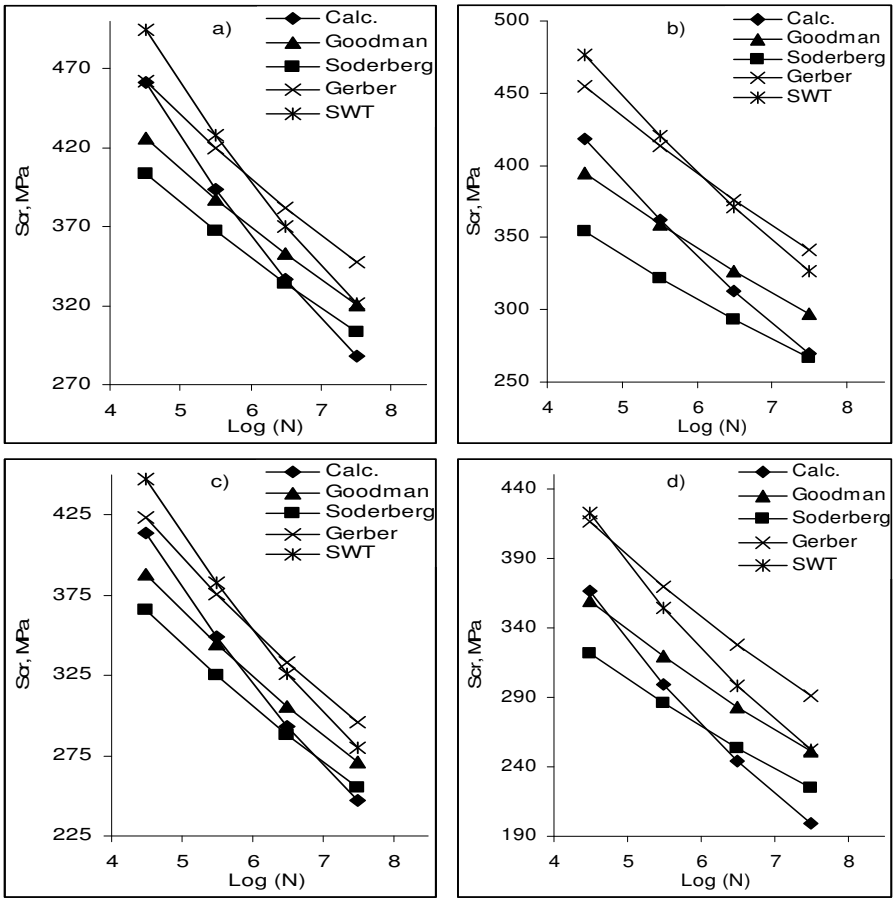

Figure 3.4 Predicted S_{cr} in case of mean stress: a – Duplok22, S_m = 70 MPa; b – Duplok22, S_m = 126 MPa; c – 3Re60, S_m = 70 MPa; d – 3Re60, S_m = 121 MPa

3.1.1 Fracture surface analysis

Fracture surface analysis performed by help of SEM revealed that fatigue crack initiation could be traced to one certain initiation point in all the tested specimens as shown in Figs. 3.5 and 3.6 (shown by arrows). It is remarkable that the appearance of fracture surfaces in case of Duplok22 and 3Re60 were quite similar despite the more homogeneous microstructure of Duplok22. In contrast Grade 5A fracture surfaces were quite rough. Striations were seen in the crack growth region and dimple fracture in the final failure zone.
Non-metallic inclusions were present in the majority of samples and the latter acted as a crack initiation point in about half of the Duplok22 samples and seemed to lower the N_f compared to those with similar stress level in absence of inclusions.

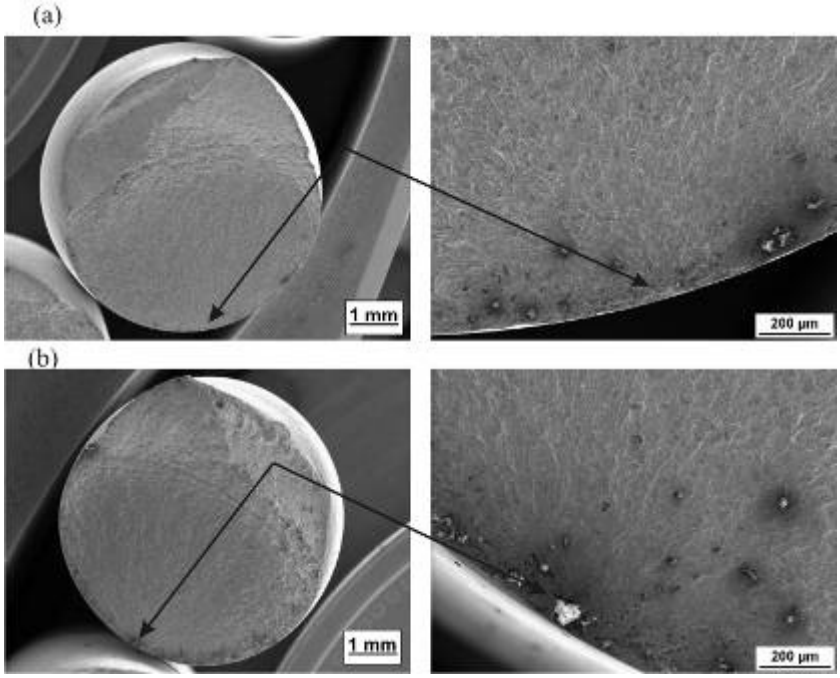

Figure 3.5 SEM images of crack initiation points of DSS Duplok22: a – 9.8×10^5 cycles, S_{mean} = 126 MPa; b – 8.6×10^4 cycles, S_{mean} = 70 MPa

This was also seen in air environment – in the majority of cases, non-metallic inclusions were found at the crack initiation point. In other half, the crack was initiated by surface irregularity, or was not clear. Small inclusions < 500 μm^2 situated near the crack initiation point, were not the initiatiators of cracks as can be seen in Fig. 3.5a. The smallest inclusions that clearly served as stress concentrators, and caused cracks to initiate were about 1250 μm^2. The largest inclusion found was 18750 μm^2 (Fig. 3.5b). In case of R = –1 inclusions with an area > 2500 μm^2, in case of S_m = 70 MPa inclusions with a size > 1250 μm^2 and in case of S_m = 126

MPa inclusions with a size > 250 μm^2 decreased the N_f. In order to evaluate the maximum inclusion size, which would allow reaching 10^7 cycles in case of Duplok22 Eq. (1.16) were used, and the inclusion size should be < 90 μm^2.

In contrast, the fracture surface analysis of 3Re60 revealed that in the majority of cases the fatigue crack started from the point without inclusions (Fig. 3.6a). Only one large inclusion was found at the initiation point in 3Re60 samples (Fig. 3.6b), even though the cycle count was pretty much the same with the specimen tested at the same stress level and with no visible inclusion.

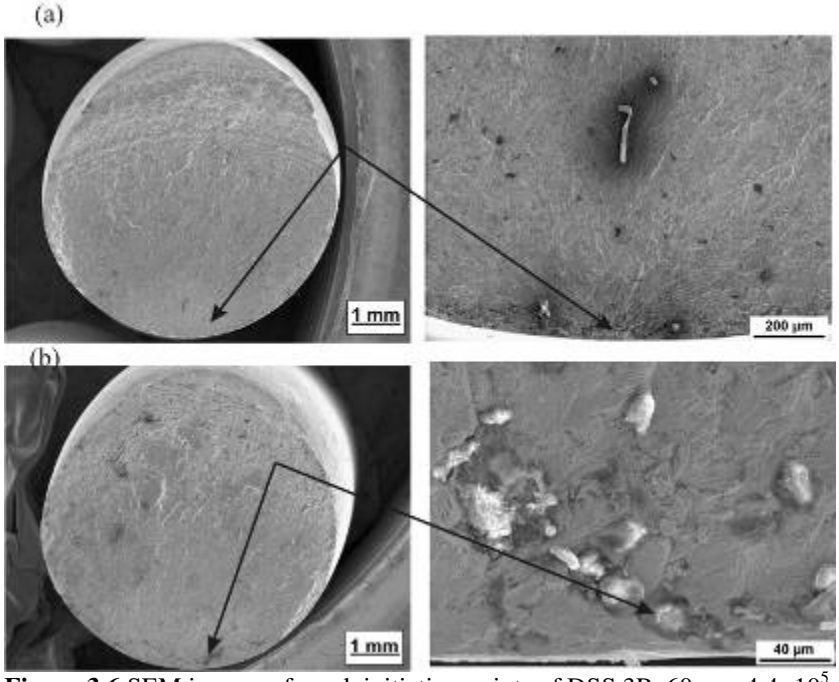

Figure 3.6 SEM images of crack initiation points of DSS 3Re60: a – 4.4×10^5 cycles, S_{mean} = 70 MPa; b – 1.6×10^6 cycles, S_{mean} = 121 MPa

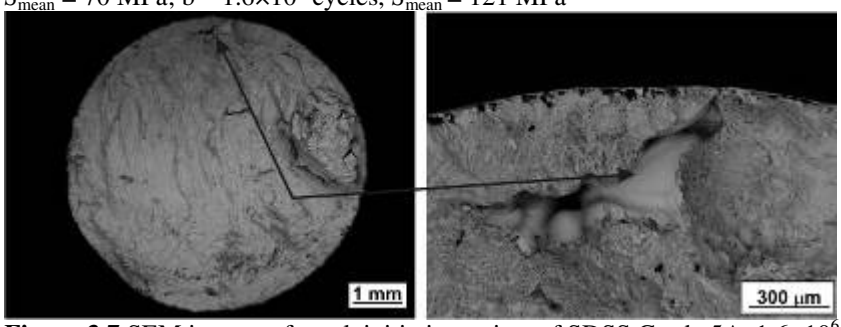

Figure 3.7 SEM images of crack initiation points of SDSS Grade 5A, 1.6×10^6 cycles, S_{mean} = 0 MPa

In case of Grade 5A, fatigue crack initiated from the surface or near surface cavities (Fig. 3.7). The crack initiation was not easily traced and it seems that there could be several initiation points. This could probably explain the lower then expected test result and the role of single inclusion seemed not to affect the fatigue strength as it was with Duplok22 or 3Re60.

As follows the effect of non-metallic inclusions on fatigue strength it is more evident in case of PM HIP-ed Duplok22. This was also concluded in [34] where stress ratio R = 0 (tension-tension loading) was used. According to our results it seems this is also the case with R = –1 and in case of the mean stress levels used in this study.

Hot rolling improves the fatigue strength by eliminating foundry defects such as cavities and should be used in case of Grade 5A.

3.2 Surface fatigue wear testing

The surface fatigue wear behaviour of the materials studied was characterized in terms of multiple wear by mass loss, and in terms of calculated volumetric wear in mm^3. However, the mass loss that occurs during the SFW test is inversely proportional to the SFW resistance of the material and the quantitative assessment of the SFW resistance is complicated. The results of SFW tests are given in Table 3.8.

Table 3.8 Surface fatigue wear of materials (pattern testing, cycle count 30 000)

Material	**Mass loss, mg**	**Volume wear, mm^3**
MMC	290.9	29.4
Weartec	5.3	0.7
Hadfield steel	17.9	2.3
Hardox 400 steel	17.8	2.3

The dependence of SFW on the number of cycles per single point (*C/P*) is given in Fig. 3.8. As it follows in the case of powder material (MMC and Weartec), the material fracture starts after a single loading to the point and the removal of material starts at low number of loading cycles (by our studies at N < 10 – 20). At the same time, for the well-known wear resistant Hadfield steel, the removal of material starts after a higher number of cycles (N ≥ 50). To find a correlation between abrasive wear and surface fatigue, the abrasive erosive wear (AEW) and abrasive impact wear (AIW) resistance of the studied materials were determined. The wear resistance of the materials studied at AEW and the AIW (3 kg abrasive) is given in Table 3.9.

To determine the correlation between AIW, AEW, SFW resistance and hardness, the corresponding diagrams were drawn (Fig. 3.9).

The relative wear resistance of the tested materials is higher in case of AIW compared to AEW. MMC has the best relative wear resistance in both cases, despite the poorest SFW test results (Table 3.9). The highest AEW and AIW

resistance of Weartec is in correlation with SFW test results (Weartec demonstrated the best result in SFW as seen in Fig. 3.9).

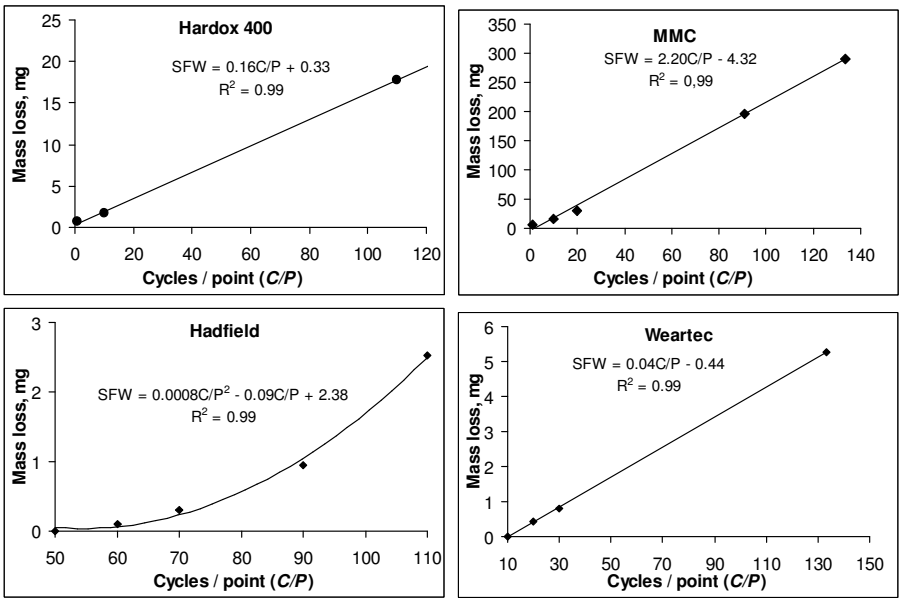

Figure 3.8 Dependence of SFW on number of loading cycles to a point

Table 3.9 Abrasive wear resistance (volumetric wear rate I_v and relative wear resistance ε_v) of studied materials

Material	**Wear resistance**			
	AEW, α = 90°		**AIW, α = 90°**	
	I_v, **mm³/kg**	ε_v	I_v, **mm³/kg**	ε_v
MMC	19.3	1.6	10.4	2.6
Weartec	30.1	1.1	11.4	2.3
Steel 45 (ref. material)	31.5	1.0	31.3	1.0
Hadfield steel	35.8	0.9	20.5	1.5
Hardox 400	26.2	1.2	39.2	0.8

To reveal the material behaviour in the conditions of SFW SEM study of worn surfaces was conducted. The wear surfaces of the PM produced MMC material and Weartec were investigated (Figs. 3.10 and 3.11).

In the conditions of SFW, the mass loss of Weartec was the least and the mass loss of MMC was the highest, exceeding others significantly. SEM images, shown in Figs. 3.10 and 3.11, explain the reasons of such behaviour. Large carbides have fractured after a single or low number of indentations, whereas cracks in the metal-matrix appear along the indentation perimeter and in the hard phase-metal matrix border. As a result, splinters or even the whole carbide particles will be removed from the contact zone. This implies that in case of SFW the load used was too high,

causing direct fracture and separation of the hard phase particles as well as cracking of the metal matrix (Fig. 3.10a and b). The matrix phase of MMC is susceptible to fatigue: the cracks eminating from the matrix can be witnessed at a high number of indentations (Fig.3.10a). Weartec, containing only small vanadium carbide particles as reinforcement (Fig 2.4b), is not as sensitive to SFW as MMC. Although some cracks can be seen on SEM micrographs of indentations already, they appear in a much later stage of the testing. Most of these cracks appear first in the VC phase, propagating later to the matrix (Fig. 3.11a). In addition to the cracks perpendicular to the surface, also the cracks parallel to the materials surface appear. Eventually, this will lead to the formation of ships and lamellas, which will be removed from the surface (Fig. 3.11b).

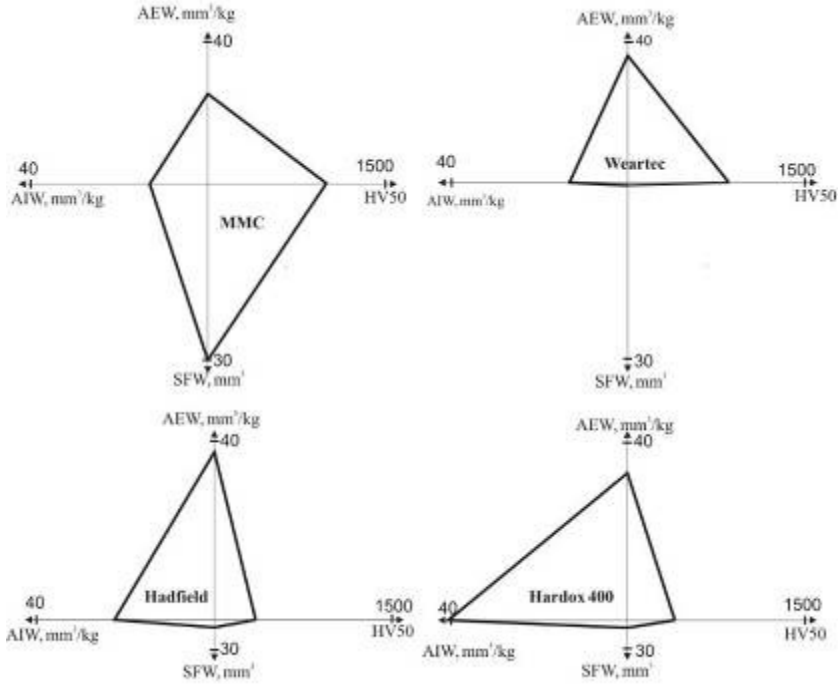

Figure 3.9 Correlation diagrams of AIW, AEW, SFW and HV for the tested materials

Although PM produced materials have high wear resistance they show higher fatigue sensitivity compared to traditional steels and the degradation starts at a low number of cycles (< 10 – 20) (Fig. 3.8) due to the fracture and separation of brittle hard phase particles (Figs. 3.10 and 3.11). The lack of correlation between abrasive erosive wear and surface fatigue wear in the current study can be most likely be explained by the difference in the scale of the loads occurring in both cases. During abrasive erosion testing processes take place in a micro scale and during surface fatigue in a macro scale. In order to have comparable results, similar scales must be used.

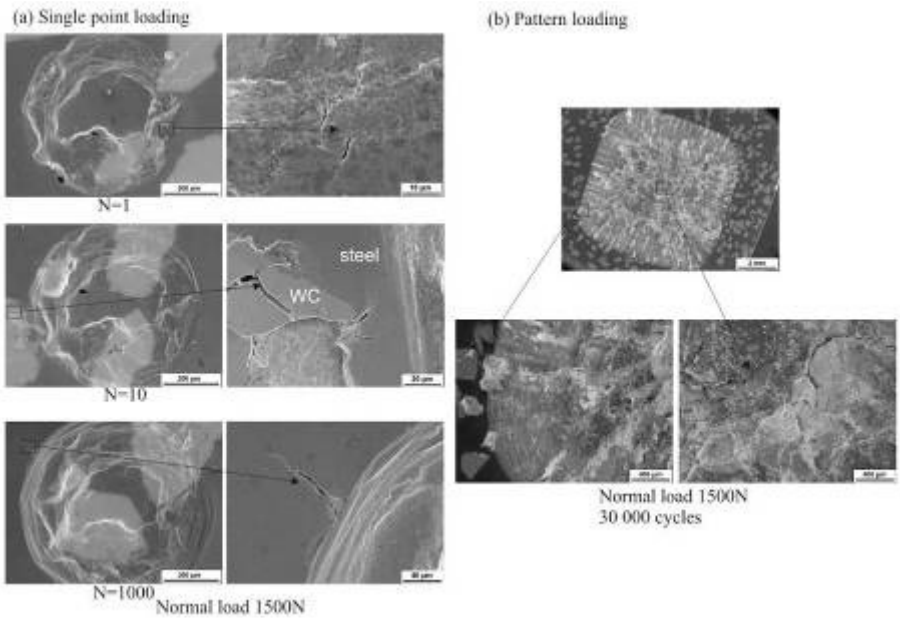

Figure 3.10 SEM images of SFW indents of MMC: a – 1, 10 and 1000 cycles per point; b – 30 000 cycles on area of 6×6 mm

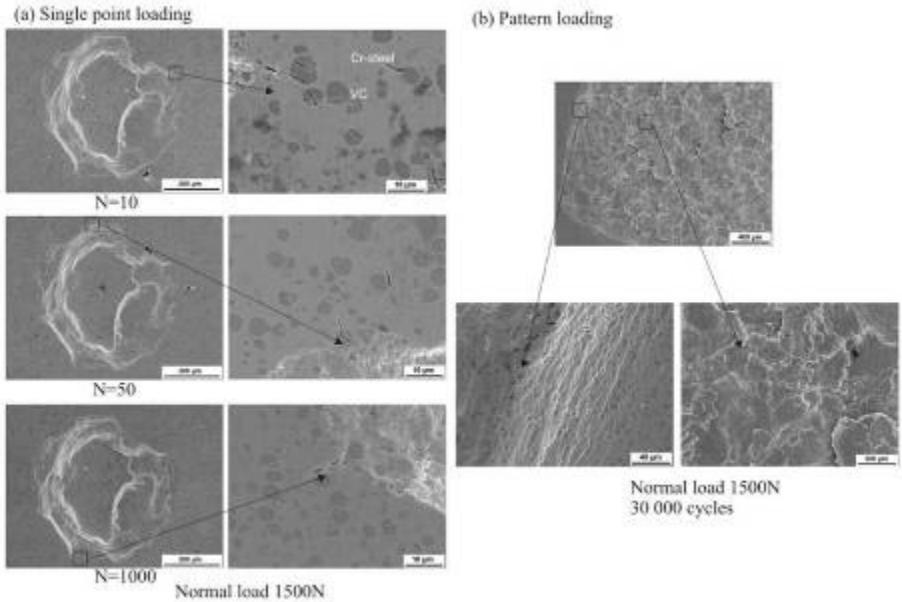

Figure 3.11 SEM images of SFW indents of Weartec: a – 1, 10 and 1000 cycles per point; b – 30 000 cycles on area of 6×6 mm

CONCLUSIONS

The main conclusions of the study on the environmental assisted fatigue of duplex steels and surface wear are as follows.

1. Powder materials – duplex steels and steel-based matrix composites are characterised by higher sensitiveness to fatigue due to the borders between different phases, non-metallic inclusions in DSS and the coarse hard phase in MMC. They act as crack initiation points and stress concentrators in heterogeneous powder materials produced by PM methods.

2. As regards corrosion fatigue:

- for prediction of the corrosion fatigue strength at 10^3 cycles, tensile strength approach is best suited;
- the best method for calculation of the fatigue limit in the air and corrosion fatigue strength at 10^7 cycles for powder steel is Duplok22 proposed by Murakami; whereas in case of cast and hot-rolled 3Re60 the best calculating result the corrosion fatigue strength at 10^7 cycles is obtained using tensile strength as a basis ($R_m/3$);
- the influence of corrosive environment on the fatigue strength becomes evident at quite an early stage, within about 10^6 cycles (about 24 hours);
- the effect of non-metallic inclusions becomes more evident with mean stress in case of PM HIP Duplok22; whereas the inclusion and surface irregularities start to play a major role at stresses exceeding 70 MPa;
- the smallest inclusions that clearly served as stress concentrators, and caused cracks to initiate were about 1250 μm^2 in case of PM HIP Duplok22;
- hot rolling improves the fatigue strength by eliminating foundry defects such as cavities and should be used in case of Grade 5A;
- commonly equations for calculating the mean stress effect did not allow predicting the corrosion fatigue strength at 10^7 cycles.

3. As regards surface fatigue:

- test results revealed that in contrast to abrasive erosion and impact wear, the wear of powder materials, however, starts in the harder phase with fracture at single or low loading cycles;
- in case of reinforced metal-matrix composite material, cracking and separation of the large harder phase plays a significant role in surface fatigue resistance;
- in comparison to traditional wear resistant Hadfield steel, surface fatigue wear starts when the number of loading cycles is one order higher;

- the abrasive-erosion and impact wear test results seem to correlate in case of powder materials and conventional wear resistant steels, but with surface fatigue due to the scale effect. It is recommended not to use the powder wear resistant materials in application where high contact stresses are prevailing and in case of dynamic surface loading.

4. Future plans:

- investigation of the role of corrosion in more detail and the possibilities of reducing its on duplex steels effect in white water environment;
- investigation of the possibility of predicting surface fatigue of coatings using indentation methods is planned as well as developing a surface fatigue testing method allowing testing surface fatigue wear and abrasive erosion in a similar scale.

REFERENCES

1. Hoeppner, W., D., *Industrial Significance of Fatigue problems*, *ASM Handbook*, Vol. 19. USA American Society for Metals, 1996

2. Stephens, I., R., Fatemi, A, Stephens, R., R., Fuchs, O., H., *Metal Fatigue in Engineering*. Second Edition. A Wiley-Interscience Publication.2001, p. 43 – 56.

3. Dowling, E., N., *Mechanical Behaviour of Materials: Engineering Methods for Deformation, Fracture and Fatigue*. 2-nd ed. Prentice Hall, 1999

4. Murakami, Y. *Metal Fatigue: Effect of small Defects and Nonmetallic Inclusions*. Elsvier, 2002

5. Perdomo, J., J, Singh, M., P., Corrosion fatigue of heat treated stainless steel in paper machine white waters, Corrosion and Materials Engineering Group, Institute of Paper Science and Technology, Atlanta, GA 303180-5794, 2002

6. Lee, Y-L., Pan, J., Hathaway, R., Barkey, M., *Fatigue Testing and Analysis*. Elsvier Butterworth-Heinmann, 2005

7. Marinelli, M., C., Degallaix, S., Alvarez-Armas, I., Short crack initiation during low-cycle fatigue in SAF 2507 Duplex stainless steel, Key Engineering Materials, 2007, p. 343 – 346

8. Kotecky, O., Degallaix, S., Polak, J., Growth of short fatigue cracks emanating from notches in an austenitic-ferritic stainless steel, *Key Engineering Materials*, 2007 Vols. 348 – 349, p. 117 – 120

9. Alvarez-Armas, I., Marinelli, M., C., Malarria, J., A., Degallaix, S., Armas, A., F., Microstructure associated with crack initiation during low-cycle fatigue in a low nitrogen duplex stainless steel, *International Journal of Fatigue,* 2007*,* Vol. 29, p. 758 – 764

10. ISO 1099:2006. Metallic materials – fatigue testing – Axial force controlled method

11. Ritchie, R., *Fatigue testing, ASM Handbook*, Vol. 8. USA American Society for Metals, 2000

12. Fatigue testing, *Encyclopedia of Materials: Science and Tecnology*, ISBN: 0-08-0431526, p. 2994 – 2998

13. Li, J., C., M., Indentation and Impression Fatigue, *Encyclopedia of Materials: Science and Technolog y,* 2001, ISBN: 0-08-0431526: p. 4042 – 4044

14. Xu, B., X., Yue, Z.,F., Wang, J., Indentation fatigue behaviour of polycrystalline copper, *Mechanics of Materials*, 2007, Vol. 39, p. 1066 – 1080

15. Alfredsson, B., Olsson, M., Initiation and growth of standing contact fatigue cracks, *Engineering Fracture Mechanics*, 2000, Vol. 65, p. 89 – 106

16. Sosnovskiy, L., A., Tribo-Fatigue, Springer-Verlag Berlin Heidelberg, 2005

17. Hokka, M., Kuokkala, V.-T., Siitonen, P., Liimatainen. J., Experimental techniques for studying the behaviour of wear resistant materials under dynamic gouging and surface fatigue, *Proc. of ICEM12-12th Intern. Conf. on Experimental Mechanics*, 2004, Politecnico di Bari, Italy

18. Sergejev, F., Antonov, M., Gregor, A., Hussainova, I., Kulu, P., Kübarsepp, J., Investigation of the surface fatigue of carbide composites and PVD coatings. *Proc. of 6th International DAAAM conference*, Tallinn, Estonia 2008

19. Sergejev, F., Investigation of the fatigue mechanics aspects of PM hardmetals and cermets, Ph. D Thesis, TUT Press, Tallinn, 2007

20. Abudaia, F.,B., Evans, J.,T., Shaw, B., A., Spherical indentation fatigue cracking, *Materials Science and Engineering,* 2005, A 391, p. 181 – 187

21. ISO 11782-: 1998. Corrosion of metals and alloys – Corrosion fatigue testing – Part 1 Cycles to failure testing

22. ISO 1099:2006. Metallic materials – fatigue testing – Axial force controlled method

23. *Encyclopedia of Materials: Science and Technology*, Elsvier, 2001

24. Jablonski, F., Varvarikes, J., Prediction of fatigue limits of surface hardened steel with regards to mean and residual stresses – A comparison, *Materials Science and Engineering*, 2007 (Article in press)

25. *Corrosion: Fundamentals, Testing and Protection*, ASM Handbook, 13a, 1996

26. Chu, C.-C., Chrenenkoff, Crack closure-based analysis of fatigue tests with mean stresses, *International Journal of Fatigue*, 2001, Vol. 23, p. 187 – 194

27. Mann, T., The influence of mean stress of fatigue crack propagation in alumimium alloys, *International Journal of Fatigue*, 2007, Vol. 29, p. 1393 – 1401

28. Kunz, L., Lukaš, P., Cyclic stress-strain behaviour of 9Cr1Mo steel at positive mean stress, *Materials Science and Engineering*, 2001, p. 555 – 558

29. Kwofie, S., An exponential stress function for predicting fatigue strength and life due to mean stresses, *International Journal of Fatigue*, 2001, Vol. 23, p. 829 – 836

30. *Uhlig's Corrosion Handbook*, Second Edition, John Wiley & Sons, Inc., 2000

31. *Metals Handbook*, Desk edition, ASTM International 1998

32. Singh, P., M., Perdomo, J., J., Oteng, J., E., Mahmood, J., Stress corrosion cracking and corrosion fatigue cracking of a duplex stainless steel in white water environments, *Corrosion, 2004,* Vol. 60, No. 9, p. 852 – 861

33. Laitinen, T, Thiosulfate pitting corrosion of stainless steels in paper machine environment, Ph. D Thesis, VTT Publications, Espoo, 1999

34. Laitinen, A, Mechanical properties, stress corrosion cracking and fatigue of powder metallurgy duplex stainless steels. Ph.D Thesis, HUT Press, Otaniemi, 1997

35. German, R. M., *Powder Metallurgy Science*, Second edition, 1994

36. *Mechanical Testing and Evaluation.* ASM handbook, 8, 2000

37. El-Yazgi, A. A., Hardie, D, *Corrosion Science*, 1998, 40, 6

38. Kotecky, O., Degallaix, S., Polak, J., Growth of short fatigue cracks emanating from notches in austenite-ferritic stainless steel. Key Engineering Materials, 2007

39. Makhlouf, K., Sidhom, H., Triguia, I., Braham, C., Corrosion fatigue crack propagation of a duplex stainless steel X6 Cr Ni Mo Cu 25-6 in air and artificial sea water, *International Journal of Fatigue*, 2003, Vol. 25, p. 167 – 179.

40. Krupp, U., Knobbe, H., Düber, O., Christ, H-J., Köster, P., Künkler, B., Fritzen, C-P,. Propagation Behaviour of Microstructually short cracks in the High-cycle and Very-high-cycle fatigue regimes. Materials Science, 2008, Vols. 567 – 568

41. Calonne, V., Gourgues, A., F., Pineau, A., Fatigue crack propagation in cast duplex stainless steels: thermal ageing and microstructural effects. Fatigue Fract. Engn. Mater. Struct., 2004,Vol. 27, p. 31 – 43

42. Batista, S., R., F., Kuri, S., E., Aspects of selective and pitting corrosion in cast duplex steels, *Anti-Corrosion Methods and Materials,* 2004, Vol. 51. No. 3, p. 205 – 208

43. Siow, K., S., Pitting corrosion of duplex stainless steels, *Anti-Corrosion Methods and Materials,* Vol. 48, No. 1, p. 31 – 36

44. Pohl, M., Storz, O., Glogowski, T., Effect of intermetallic precipitations on the properties of duplex stainless steel, *Materials Characterization*, 2007, p. 65 – 71

45. Ezuber, H., M., El-Houd, A., El-Shawesh, F., Effects of sigma phase precipitation on seawater pitting of duplex stainless steel, *Desalination,* 2007, p. 268 – 275

46. Lo, I-Hsuang, Tsai W., T., Effect of selective dissulution on fatigue crack initiation in 2205 duplex stainless steel, *Corrosion Science,* 2007,Vol. 49, p. 1847 – 1861

47. Cvijovic, Z., Radenkovic, G., Microstructure and pitting corrosion resistance of annealed duplex stainless steel, *Corrosion Science*, 2006, Vol. 48, p. 3887 – 3906

48. Utrilla, M., V., Urena, A., Munez, C., J., Influence of heat treatmenst on the corrosion resistance of a duplex stainless steel manufactured by powder metallurgy, *Corrosion,* 2006, Vol. 62, No. 1, p. 84 – 89

49. Young, M., C., Tsay, L., W., Shin, C.-S., Chan, S., L., I., The effect of short time post-weld heat treatment on the fatigue crack growth of 2205 duplex stainless steel welds, *International Journal of Fatigue,* Vol. 29, 2007, p. 2155 – 2162

50. Kulu, P., Selection of powder coatings for extreme erosion wear conditions Advanced Engineering Materials, 2002, 4, No. 6

51. Terheci, M., Microscopic investigation on the origin of wear by surface fatigue in dry sliding*, Materials Characterization,* Vol. 45, p.1 – 15

52. Kleis, I., Kulu, P., *Solid Particle Erosion. Occurrence, Prognostification and Control*, TUT Press, 2005

53. Veinthal, R., Characterization and Modelling of Erosion Wear of Powder Composite Materials and Coatings, Ph.D Thesis, TUT Press, Tallinn, 2005

54. Veinthal, R., Kulu, P., Käerdi, H., Characterization of the structure of composite powder materials and coatings, *Materials Science (Medžiagotyra),* 2005, Vol. 11, No. 4

55. Preis, I., Fatigue Performance and Mechanical Reliability of Cemented Carbides, Ph. D Thesis, TUT Press, Tallinn, 2004

56. EVS-EN 10002-1. Metallic materials – Tensile testing – Part 1: Method of test at ambient temperature

57. EVS-EN ISO 6507-1:2006. Metallic materials - Vickers hardness test – Part 1: Test method

58. Laaneots, R., Mathiesen, O., Mõõtmise alused, TUT Press, 2002

59. www.metsopaper.com/MP/Marketing/mpv2store.nsf/BYWID/WID-030915-2256C-309D9/$File/32020_V2_EN.pdf?openElement (15.06.08)

60.http://www.outokumpu.com/pages/fsOpenDocument.htm?url=http://www.outokumpu.com/pages/Page____7742.aspx?docid=241142 (15.06.08)

LIST OF PUBLICATIONS

Main publications

Paper I
Saarna, M. Fatigue of duplex steels in synthetic white water environment *Powder Metallurgy Progress*, 2006, Vol.6, No. 3, p. 142–145

Paper II
Saarna, M., Peetsalu, P. Effect of mean stress on fatigue strength of duplex steels in synthetic white water environment, *Proc. of 6th International DAAAM Baltic Conference "INDUSTRIAL ENGINEERING",* 24–26 April 2008, Tallinn, Estonia, p. 531–536 (ISBN 978-9985-59-783-5)

Paper III
Saarna, M., Kulu, P., Veinthal, R., Tarbe, R. Study of surface fatigue of wear resistant powder materials, *Proc. Estonian Sci. Eng*., 2006, Vol. 12, No. 4, p. 377–387

Paper IV
Kulu, P., Veinthal, R., **Saarna, M**. Tarbe, R. Surface fatigue processes at impact wear of powder materials, *Wear,* 2007, p. 463–471

Approbation and conference papers

1. Saarna, M. Laansoo, A. Rail and rail weld testing, *Proc. 4th International DAAAM Conference "INDUSTRIAL ENGINEERING – INNOVATION AS COMPETITIVE EDGE FOR SME"* 2004, Tallinn, Estonia, p. 223–225 (ISBN 9985-894-59-6)

2. Laansoo, A., Kübarsepp, J., Saarna, M., Klaasen, H. Internal stresses in diffusion bonded joints, *Materials Science (Medžiagotyra*), 2005, Vol. 11, No. 4, p. 110–113

3. Saarna, M. Fatigue of duplex steels in corrosive environment, *4th International DAAAM Conference "INDUSTRIAL ENGINEERING – INNOVATION AS COMPETITIVE EDGE FOR SME"*, 2006, Tallinn, Estonia, p. 289–293 (ISBN 9985-894-92-8)

4. Peetsalu, P., Saarna, M., Mikli, V., Juurma, M., Computer based steel microstructure analysis describing the size and distribution of structure phases, *Proc. of 13th International Symposium on Metallography "METALLOGRAPHY 2007"* 2nd–4th May 2007, Stará Lesná, Slovakia, p. 91–95

5. Peetsalu, P., Saarna, M., Mikli, V., Assesment of non-metallic inlusions in sheet metals by computer analysis, *7th International Conference on Clean Steel,* 2007, Hungary

Author's contribution in the main publications

In Papers I and II the author was responsible for the sample preparation, testing, collecting and analysis as well as publication of the test data. In Papers III and IV the author conducted surface fatigue tests, data collecting and analysis, took part in discussion and was involved in co-writing of the publications.

ABSTRACT

Among the powder materials, duplex stainless steels and steel-based metal-matrix composite materials are used in a wide range of applications and conditions where corrosion, wear and fatigue are prevailing. In many cases, failure of components manufactured from these materials is due to the severity of working in the above-mentioned conditions.

The aim of the present work is to study the fatigue caused by the environment and by indentation. In case of duplex stainless steels (DSS), traditional fatigue strength assessment methods were analysed. The aim of the latter was to predict corrosion fatigue strength of DSS, produced in powder metallurgy (PM), in synthetic white water environment. It was observed that Murakami method based on hardness was suitable for the powder DSS, while for traditional as cast, cast and hot-rolled DSS, the best-suited method was based on tensile strength. Corrosion fatigue testing was performed in conditions of tension-compression and in synthetic white water environment. The variables were the alternating stress level S_{alt}, and count of output cycles. The S_{alt} values were chosen to cover the S-N curve from 10^4 to run out (10^7) cycles.

Wear resistant materials from powder steel-based metal matrix composites (MMC) wear resistant materials were studied in conditions of abrasive, erosive and impact wear, as well as of those of surface fatigue wear. The purpose of the latter was to evaluate the role of surface fatigue in the wear process. The results showed that the mechanisms of material removal are different as compared to traditional and powder materials.

Keywords: duplex stainless steel, steel-matrix-based wear resistant materials, corrosion fatigue, surface fatigue, abrasive erosion, impact wear

KOKKUVÕTE

Tihti on masinate ja nende komponentide enneaegne purunemine seotud kulumise ja väsimusega. Paljudel juhtudel on tegemist mitmete purunemiseni viivate protsesside koosmõjuga: kulumine-korrosioon, väsimus-korrosioon, väsimus-kulumine. Nendest protsessidest tekkivate kahjude vältimine on olnud viimastel aastatel aktuaalne. Suundumised tehnomaterjalide valdkonnas Euroopas on toodud nn. Tehnoloogiaplatvormides. Ühes neist, tehnoloogiaplatvormis EuMAT on esile tõstetud muuhulgas uute materjalisüsteemide arendamise vajadus, samuti ka vajadus materjalide degradatsioonimehhanismide väljaselgitamiseks. Praeguseks ajaks on välja töötatud rida materjale, mille kasutuselevõtt võimaldab pakkuda uusi lahendusi ja tõsta seadmete tootlikkust.
Roostevabad terased on ennast tõestanud korrosiivsetes keskkondades, nende hulgas on ennast õigustanud ka suurepärase korrosioonikindlusega roostevabad dupleksterased. Seda just paberitööstuses oma heade tugevus- ja korrosioonikindluse näitajate tõttu. Dupleksteraste töökindlust agressiivsetes keskkondades saab veelgi parandada läbi legeerivate elementide osakaalu suurendamise ja struktuuri ühtlustamise – seda võimaldab pulbermetallurgia tehnoloogia kasutamine roostevabade dupleksteraste tootmisel. Seega on aktuaalne sellisel teel valmistatud roostevabade pulberdupleksteraste uurimine väsimuse ja korrosiooni koosmõju tingimustes.
Tribomaterjalide puhul on perspektiivsed heterogeense struktuuriga materjalid – kõvafaasi osakesed seotuna suhteliselt pehmes maatriksis. Abrasiivkulumise tingimustes eelistatakse metall-maatriksiga komposiitmaterjale. Selliseid karbiide sisaldavaid materjale valmistatakse reeglina pulbermetallurgilisi või pihustusmeetodeid kasutades. See heterostruktuur tagab nendel materjalidel kõrge abrasiivkulumiskindluse. Kuid samas on terve rida rakendusi, kus sellest ei piisa, nagu näiteks löök- ja tsüklilise koormamise tingimused. Sellisel juhul muutub määravaks ka seda tüüpi kulumiskindlate materjalide pinnaväsimusomadused. Viimaseid aga ei ole piisavalt uuritud.

Ülevaatest tulenevalt oli käesoleva töö eesmärkideks püstitatud uurida väsimusprotsesse pulberteraste korral ja sellest tulenevalt anda soovitusi nende materjalide kasutamisel.

Roostevaba pulberterase korral oli eesmärkideks:

- selgitada korrosiivse keskkonna mõju pulberdupleksterase väsimusele ja võrrelda seda roostevabade tavadupleksteraste omadega;
- uurida võimalusi korrosioonväsimustugevuse prognoosimiseks roostevabade pulber- ja tavadupleksteraste puhul;
- hinnata korrosiivse keskkonna ja keskpingete koosmõju pulberterase väsimustugevusele.

Kulumiskindlate pulbermaterjalide korral oli eesmärgiks:

- uurida pulberteraste kulumiskindlust erinevates abrasiivkulumise tingimustes;
- selgitada pulberkomposiitmaterjalide kulumise mehhanisme ja pinnaväsimuse vahelisi seoseid abrasiivsel erosioon- ja löökkulumisel.

Töö eksperimentaalses osas uuriti roostevaba duplekspulberteraste väsimustugevust teljesihilise tõmbe-surve olukorras. Väsimustugevust uuriti madal- ja kõrgtsüklilisel koormamisel korrodeeruvas keskkonnas (vastava tsüklite arvuga alates 10^4 kuni 10^7) ning koostati antud kui ka traditsiooniliste valatud dupleksteraste väsimuskõverad. Eraldi tähelepanu all oli korrosiooni mõju väsimusomadustele. Selgitati välja keskpingete mõju pulberterase väsimusomadustele. Selgus, et mittemetalsed lisandid mängivad olulist rolli pulberterase väsimustugevusel. Püüti prognoosida materjalide väsimustugevust, kasutades erinevate autorite poolt väljapakutud empiirilisi valemeid ning materjalide tugevusomadusi.
Eraldi tähelepanu all olid murdepinnad, selgitamaks välja väsimusprao tekke põhjused ja selle arenemine. Uuringutest selgus, et reeglina algab väsimusprao teke materjali pinnal või pinna läheduses olevatest mittemetalsetest lisanditest.
Kulumiskindlate pulbermaterjalide pinnaväsimust uuriti indenteerimise teel. Terasmaatriksiga pulbermaterjalide korral uuriti materjalide kulumise mehhanismi ja kulumiskindlust abrasiivse erosioon- ja löökulumise tingimustes. Selgitati välja seosed materjalide abrasiivkulumiskindluse ja pinnaväsimuse vahel. On koostatud diagrammid materjalide kõvaduse, erosioon- ja löökulumise ning pinnaväsimuse vaheliste seoste kohta. Erinevalt traditsioonilistest kulumiskindlatest terastest (nt. Hadfieldi teras) on pulberterastele omane suur tundlikkus väsimusele – vaatamata terasmaatriksiga pulberkomposiitmaterjalide heale kulumiskindlusele leiab väsimusdegratatsioon aset juba väikeste tsüklite arvu ($< 10 - 20$) korral. Suurt erinevust pulberkomposiitmaterjalide abrasiivse erosioon- ja löökulumise ning väsimuse vahel saab eelkõige selgitada mastabiefektiga: erosioon- ja löökkulumisel on tegemist eelkõige mikroskaalal protsessidega, pinnaväsimuse korral aga nähtusega makroskaalal. Seega tuleb pulberkomposiitmatejalide puhul vältida selliseid tööolukordi, kus on tegemist suurte kontaktpingetega ja dünaamilise kormusega.

Tulemused ja järeldused

1. Pulberteraste korrosioonväsimusel:
   - duplekspulberterase Duplokk22 omab roostevaba tavadupleksterase ees märgatava eelist oma homogeense struktuuri tõttu;
   - korrosioonväsimustugevuse hindamisel saab töös kasutatud korrosiivsekeskkonna ja koormamissageduse puhul Duplok22 korral kasutada Murakami kõvadusel põhinevat meetodit, samas kui tavadupleksteraste

puhul väsimustugevuse hindamisel korrosiivses keskkonnas on sobivaim aga tugevuspiir;

- Duplok22 puhul suurema kui 70 MPa keskpingeväärtuse puhul saab lisaks korrosiivsele keskkonnale määravaks pinnal või pinna läheduses olevad mittemetalsed lisandid;

2. Terasmaatriksiga pulberkomposiitmaterjalide pinnaväsimusel:
   - väsimus-kulumise tingimustes saab kõvafaasi osakesi sisaldava kulumiskindla materjali kulumine alguse kõvema ja haprama faasi pragunemisest ühekordse või väikesearvuliste koormamistsüklite tagajärjel;
   - metallmaatrikskomposiidi kulumiskindluse juures mängib põhirolli karbiidse faasi pragunemine ning järgnevalt selle eraldumine juba väikeste tsüklite arvu korral, samas on Hadfieldi terase puhul materjali eraldumine pinnast on seotud suurusjärgu suurema koormamistsüklitega, mis on seletatav selle terase suurema sitkusega ja plastsusega;
   - kulumiskindlate pulbermaterjalide tulemused korreleeruvad abrasiivse erosioon- ja löökkulumise tingimustes, mitte aga pinnaväsimustugevusega kuna toimuvatel portsessidel mõjuvate jõudude suurusjärgud on erinevad.

CURRICULUM VITAE

1. Personal data

Name	Mart Saarna
Date and place of birth	16.12.1978

2. Contact information

Address	Ehitajate tee 5, 19086, Tallinn Estonia
Phone	+372 620 3353; +372 55 904 386
E-mail	mart.saarna@ttu.ee

3. Education

Educational institution	**Graduation year**	**Education (field of study/degree)**
Tallinn University of Technology	2007	Production Engineering/ MSc.
Tallinn University of Technology	2002 –	Mechanical and instrumental engineering/ PhD student
Tallinn University of Technology	2002	Production Engineering/ MEng.
Tallinn University of Technology	2001	Production Engineering/ BSc.

4. Language competence/skills (fluent; average, basic skills)

Language	**Level**
Estonian	mother tongue
English	average
Finnish	basic skills
Russian	basic skills

5. Special Courses

Period	**Educational or other organisation**
2006	Powder metallurgy training courses, European Powder Metallurgy Association (EPMA)
2002	Course on non-destructive testing. Visual testing (II level)
2000	Course on non-destructive testing. Penetrant and magnetic particle testing (II level)

6. Professional Employment

Period	**Organisation**	**Position**
2004 –	Tallinn University of Technology, Faculty of Mechanical Engineering, Department of Materials Engineering, Chair of Materials engineering	Teaching assistant
2002 – 2004	Tallinn University of Technology, Faculty of Mechanical Engineering, Department of Materials Engineering, Chair of Materials Science.	Researcher
2001 –	Laboratory of Mechanical Testing and Metrology of Tallinn University of Technology	Expert
2000 – 2002	Tallinn University of Technology, Faculty of Mechanical Engineering, Department of Materials Engineering, Chair of Materials Science.	Engineer

7. Defended theses

The examination methods for determining of non-metallic inclusions and micro structure in duplex stainless steel, Bachelor`s degree, *Priit Schultz*.

8. Main areas of scientific work/Current research topics

Fatigue characteristics of steels and wear resistant materials and coatings.

9. Other research projects

Effect of mean stress on fatigue strength of duplex stainless steel. Engineering Purchase Contract No. V244 Metso Powdermet OY and Tallinn University of Technology, 2004 – 2006.

Targeted financed projects

SF 014050502 Wear resistant materials and wear, 2006 – 2007.

SF 014009108 Hard coatings and surface technology, 2008 – 2013.

ELULOOKIRJELDUS

1. Isikuandmed

Ees- ja perekonnanimi	Mart Saarna
Sünniaeg ja -koht	16.12.1978, Tallinn, Eesti
Kodakondsus	eestlane

2. Kontaktandmed

Aadress	Ehitajate tee 5, 19086, Tallinn
Telefon	+372 620 3353; +372 55 904 386
E-posti aadress	mart.saarna@ttu.ee

3. Hariduskäik

Õppeasutus (nimetus lõpetamise ajal)	**Lõpetamise aeg**	**Haridus (eriala/kraad)**
Tallinna Tehnikaülikool	2007	Tootmistehnika, MSc.
Tallinna Tehnikaülikool	2002 –	Masina ja aparaadiehitus, Doktoriõpe
Tallinna Tehnikaülikool	2002	Tootmistehnika, MEng.
Tallinna Tehnikaülikool	2001	Tootmistehnika, BSc

4. Keelteoskus (alg-, kesk- või kõrgtase)

Keel	**Tase**
Eesti	emakeel
Inglise	kesktase
Soome	algtase
Vene	algtase

5. Täiendusõpe

Õppimise aeg	**Täiendusõppe läbiviija nimetus**
2006	Suvekool pulbermetallurgias, Euroopa pulbermetallurgia ühing (EPMA)
2002	Mittepurustava kontrolli kursus. Visuaalkontrolli meetod II tase. Inspecta OY Soome
2000	Mittepurustava kontrolli kursus. Kapillaar- ja magnetpulbermeetod II tase. AEL OY, Inspecta OY Soome

6. Teenistuskäik

Töötamise aeg	Tööandja nimetus	Ametikoht
2004 –	Tallinna Tehnikaülikool, Mehaanikateaduskond, Materjalitehnika instituut, metallide tehnoloogia õppetool.	Assistent
2002 – 2004	Tallinna Tehnikaülikool, Mehaanikateaduskond, Materjalitehnika instituut, Materjaliõpetuse õppetool.	Teadur
2001 –	Tallinn Tehnikaülikool, Mehaanika ja metroloogia katselabor	Metallide katseala ekspert
2000 – 2002	Tallinna Tehnikaülikool, Mehaanikateaduskond, Materjalitehnika instituut, materjaliõpetuse õppetool.	Insener

7. Teadustöö põhisuunad

Teraste ja kulumiskindlate materjalide väsimuskarakteristikud.

8. Kaitstud lõputööd

Mittemetalsete lisandite ja metalse põhimassi struktuuri määramise metoodika dupleks roostevabas terases, Bakalaureuse töö, *Priit Schultz.*

9. Teised uurimisprojektid

Välisleping V244 "Effect of mean stress on fatigue strength of duplex stainless steel" Metso Powdermet OY ja Tallinna Tehnikaülkool, 2004-2006.
Sihtteema SF 0140505 Kulumiskindlad materjalid ja kulumine, 2006 – 2008.
Sihtteema SF 014009108 Kõvapinded ja pinnatehnika, 2008 – 2013.